Systematic survey of phosphate materials for lithium-ion batteries by first principle calculations

(第一原理計算によるリチウムイオン電池用リン酸塩材料の系統的探索)

Koji OHIRA

Index

Chapter 1
General Introduction

1-1 Introduction

In recent years, demands for the natural and renewable energy sources such as photovoltaic power and wind power continue to increase. The demands grow even more rapidly after the nuclear accident in Fukushima, Japan in March 2011. However supplies of these natural energy sources are strongly dependent on natural conditions. Massive rechargeable batteries are therefore required for balancing the power supplies and demands. Depending on the application, many technical requirements should be met for the rechargeable batteries, They are required to be high-energy density, high-power density, high safety, low cost , just to mention a few requirements. The rechargeable batteries include lead-acid battery, nickel cadmium battery, nickel metal hydride battery and lithium-ion battery [1] [2]. The advantages of the lithium-ion battery are high-energy density, high-power density, low self-discharge and high efficiency between charge and discharge. Therefore lithium-ion battery

is thought to be most promising among currently available battery systems.

In the present study, we performed the systematic survey of phosphate materials for lithium-ion batteries by first principles calculations.

This paper is organized as follow:

In chapter 1, we described the general introduction of lithium-ion battery. Especially we explain the cathode materials and first principle calculations for lithium-ion batteries and exploring a new material.

In chapter 2, we reported the phase relationships in pseudo-ternary systems of $1/2Li_2O$-MO-$1/2P_2O_5$ and $1/2Li_2O$-$1/2M_2O_3$-$1/2P_2O_5$ (M = Mg, Ti to Zn). In each composition, the formation energy was calculated by first principle calculations and the calculation results compared to the ICSD.

In chapter 3, we conducted the comparative study of crystal structures of lithium metal phosphates. We attempted to comprehend the relationship among the coordination number, bond length, cell volume and ratio of phosphorus to cation.

In chapter 4, we conducted the comparative study of battery voltage of lithium metal phosphates. This study focused on relationship to the cell volume of each structure.

1-2 Lithium-ion battery

Lithium-ion batteries consist of three main components such as

cathode, anode and electrolyte. Generally, the cathode is a metal oxide [3] and the anode is a carbon [4]. The electrolyte is a lithium salt in an organic solvent. The properties of lithium-ion batteries are related closely to the selected materials.

In lithium-ion batteries, the basic reaction is the transfer of lithium ions between cathode and anode. During a charging, lithium ions are extracted from the cathode materials and inserted into anode materials. During a discharging, this electrochemical reaction is the reverse process. The chemical reactions for charge and discharge are shown as below.

$$\text{Cathode :} \quad LiMO_2 \underset{\text{Discharge}}{\overset{\text{Charge}}{\rightleftharpoons}} Li_xMO_2 + xLi^+ + xe^-$$

$$\text{Anode :} \quad C + xLi^+ + xe^- \underset{\text{Discharge}}{\overset{\text{Charge}}{\rightleftharpoons}} Li_xC$$

$$\text{Battery as a whole :} \quad Li_xMO_2 + C \underset{\text{Discharge}}{\overset{\text{Charge}}{\rightleftharpoons}} MO_2 + Li_xC$$

The disadvantage of lithium-ion batteries is safety risk. If lithium-ion batteries become overheated or overcharged, the lithium-ion batteries have been known to exhibit thermal runaway and explode [5-8]. To reduce these risks, lithium-ion battery packs contain fail-safe circuitry.

Furthermore other safety features are required in each battery.

1-3 Cathode materials for lithium-ion batteries

Three types of structures are known as cathode materials. One structure is the layered structure such as a lithium cobalt oxide [9]. The cathode materials with layered structure have a high energy density and low thermal stability [10]. Another structure is spinel structure such as a lithium manganese oxide [11] [12]. The cathode materials with spinel structure have a lower energy density and higher thermal stability than the cathode materials with layered structure [13]. The other structure is the olivine structure such as a lithium iron phosphate [14]. The cathode materials with olivine structure have a high thermal stability [15] [16].

Cathode materials are required to be high-energy density, high-power density, high safety, low cost, just to mention a few requirements. However high-energy density and high safety cannot be satisfied.

The theoretical capacity of these cathode materials is calculated the following equation (1).

$$Q = \frac{nF}{M \times 3600} \qquad (1)$$

Q is theoretical capacity typically given in the unit of Ah/g. F is the Faraday constant, n is the charge transported and M is molecular weight.

The voltage is calculated by the chemical potential difference between

cathodes and anodes. The voltage E is calculated from the following formula (2) [17] [18].

$$E = -\frac{\mu_{\mathrm{Li}}^{\mathrm{cathode}} - \mu_{\mathrm{Li}}^{\mathrm{anode}}}{zF} \qquad (2)$$

F is the Faraday constant and z is the charge transported. If chemical potential of cathode materials increase, the battery voltage is increasing. Hence energy density can increase. However cathode materials with a high chemical potential cannot use because electrolytes do not exist. Therefore it is necessary to develop the optimum cathode materials.

1-4 First principle calculations for lithium-ion batteries

First principle calculations for lithium-ion batteries have two types of approach. First the first principle calculations were used for to explain the experimental results [19-23]. These calculations shed light on a chemical reaction. Second the first principle calculations were used for to search a new material. This approach was attempt at constructing a phase diagram [24-26] and calculated voltage [27] [28]. Unfortunately, these calculations do not always guarantee that calculation results are consistent with experimental results.

Materials informatics has been much attention in recent years [29] [30]. The concept of materials informatics is to apply the principle of

informatics to the material science. Materials informatics is the promising approach to discover a new material. Materials informatics needs a massive database and data mining technique. It believed that first principle calculations are important skills to make a massive database. High-throughput calculations were performed for exploring a new material in lithium-ion batteries [31] [32].

References

[1] K. Ozawa, Solid State Ionics, 69, 212-221 (1994)

[2] S. Megahed and B. Scrosati, J. Power Sources, 51, 79-104 (1994)

[3] K. Mizushima, P.C. Jones, P.J. Wiseman and J.B. Goodenough, Mater. Res. Bull., 15, 783-789 (1980)

[4] Z. X. Shu, R. S. McMillan and J. J. Murray, J. Electrochem. Soc., 140(4), 922-927(1993)

[5] R. A. Leising, M. J. Palazzo, E. S. Takeuchi and K. J. Takeuchi, J. Power Sources, 97–98, 681-683 (2001)

[6] T. Ohsaki, T. Kishi, T.Kuboki, N. Takami, N. Shimura, Y. Sato, M. Sekino and A. Satoh, J. Power Sources, 146(1–2), 97-100 (2005)

[7] Q. Wang, P. Ping, X. Zhao, G. Chu, J. Sun and C. Chen, J. Power Sources, 208(15), 210-224 (2012)

[8] S. Tobishima amd J. Yamaki, J. Power Sources, 81–82, 882-886 (1999)

[9] T. Ohzuku, A. Ueda, and M. Nagayama, J. Electrochem. Soc., 140(7), 1862-1870 (1993)

[10] Y. Baba, S. Okada and J. Yamaki, Solid State Ionics, 148(3–4), 311-316 (2002)

[11] T. Ohzuku, M. Kitagawa, and T. Hirai, J. Electrochem. Soc., 137(3), 770-775 (1990)

[12] D. Guyomard and J. M. Tarascon, J. Electrochem. Soc., 139(4), 937-948 (1992)

[13] M.M. Thackeray, M.F. Mansuetto, D.W. Dees and D.R. Vissers, Mat. Res. Bulletin, 31(2), 133-140 (1996)

[14]A.K.Padhi, K.S.Nanjundaswamy and J. B. Goodenough, Electrochem. Soc., 144(4), 1188-1194 (1997)

[15] A. S. Andersson,a, J. O. Thomas, B. Kalska and L. Häggströmb, Electrochem. and Solid-State Lett., 3(2), 66-68 (2000)

[16] M. Takahashi, H. Ohtsuka, K. Akuto and Y. Sakurai. Electrochem. Soc., 152(5), A899-A904 (2005)

[17] G. Ceder, M.K. Aydinol and A.F. Kohan, Comp. Matr. Sci., 8(1–2) 161-169 (1997)

[18] Y. Koyama, I. Tanaka, Y. Kim, S. R. Nishitani, and H. Adachi, J. Appl. Phys., 38, 4804–4808 (1999)

[19] M. Nakayama, M. Kaneko and M. Wakihara, Phys. Chem. Chem. Phys., 14, 13963–13970 (2012)

[20] Y. Koyama, I. Tanaka, M. Nagao and R. Kanno, 214th ECS Meeting

[21]Y. Koyama, H. Arai, I. Tanaka, Y. Uchimoto and Z. Ogumi, Chem. Matr., 24(20), 3886-3894 (2012)

[22] Y. Okamoto, J. Electrochem. Soc., 159(2), A152-A157 (2012)

[23] D. Morgan, A. Van der Ven and G. Ceder, Electrochem. Solid-State Lett., 7(2), A30-A32 (2004)

[24] A. Van der Ven, M. K. Aydinol, and G. Ceder, Phys. Rev. B, 58, 2975–2987 (1998)

[25] S. P. Ong, L. Wang, B. Kang, and G. Ceder, Chem. Mater., 20(5),

1798-1807 (2008)

[26] R. E. Doe, K. A. Persson, Y. S. Meng and G. Ceder, Chem. Mater., 20, 5274–5283 (2008)

[27] T. Mueller, G. Hautier, A. Jain, and G. Ceder, Chem. Mater., 23, 3854–3862 (2011)

[28] M. Cococcioni, C. A. Marianetti, D. Morgan, and G. Ceder, Phys. Rev. B, 70, 235121 (2004)

[29] S. Curtarolo, D. Morgan, K. Persson, J. Rodgers and G. Ceder, Phys. Rev. Lett., 91, 135503 (2003)

[30] R. Jalem, T. Aoyama, M. Nakayama and M. Nogami, Chem. Mater., 24, 1357−1364 (2012)

[31] G. Hautier, A. Jain, H. Chen, C. Moore, S. P. Ong and G. Ceder,.J. Mar. Chem., 21, 17147-17153 (2011)

[32] T. Mueller, G. Hautier, A. Jain and G. Ceder, Chem. Mater., A-I (2011).

Chapter 2

Phase relationships in pseudo-ternary systems of $1/2Li_2O$-MO-$1/2P_2O_5$ and $1/2Li_2O$ -$1/2M_2O_3$-$1/2P_2O_5$ (M = Mg, Ti to Zn)

2-1 Introduction

Lithium transition metal phosphates for lithium-ion batteries have received much attention in recent year due to their higher safety and better cycling stability than other kinds of cathode materials. These properties are important because lithium-ion batteries are used not only for portable devices, such as mobile phone and notebook computer, but also for large-scale devices. The large-scale devices include batteries for electric vehicles and large-scale energy storage systems used for the grid energy storages.

Some of lithium metal phosphates were reported as cathode materials, anode materials and solid states electrolytes for lithium-ion batteries. For example, $LiFePO_4$ [1-3], $LiMnPO_4$ [4], $LiCoPO_4$ [5], $Li_2FeP_2O_7$ [6] and $Li_3V_2(PO4)_3$ [7] were reported as cathode materials. $Sn_2P_2O_7$ [8] was reported as anode materials. $LiTi_2(PO_4)_3$ [9] was reported as solid state

electrolytes. Especially the $LiFePO_4$ cathode material has received much attention in recent year due to their high safety and excellent cycling stability [10] [11].

Some of the lithium metal phosphates were also studied by first principle calculations. The research group of Ceder calculated phase stability, lithium conductivity, polaron migration, voltage, surface properties and some other properties [12-27]. Some phase diagrams are now available on the open website of “Material Project”. These previous works attempted to shed light on a chemical reaction and to explore a new material. Unfortunately, these calculations do not always guarantee that calculation results are consistent with experimental results. Therefore it was difficult to use for exploring new materials.

However materials informatics has been much attention in recent years [28-32]. The concept of materials informatics is to apply the principle of informatics to the material science. Materials informatics is the promising approach to discover a new material. Materials informatics needs a massive database and data mining technique. It believed that first principle calculations are important skills to make a massive database.

The purpose of this study was to describe phase relationships in pseudo-ternary systems and to compare calculation data to experimental data. This comparative study aimed to examine the formation energies of compounds contained in the ICSD.

2-2 Method

The current study involved investigating phase relationships and comparing calculation data to experimental data. Formation energies were calculated by phase relationships in pseudo-ternary systems of $1/2Li_2O$-MO-$1/2P_2O_5$ and $1/2Li_2O$-$1/2M_2O_3$-$1/2P_2O_5$. The calculation results were compared to experimental data. The formation energies of crystal structures contained in the ICSD were examined by first principle calculations.

The phase relationships in pseudo-ternary systems of $1/2Li_2O$-MO-$1/2P_2O_5$ and $1/2Li_2O$-$1/2M_2O_3$-$1/2P_2O_5$ were examined by first principle calculations. The divalent elements were selected from Mg, Ti, V, Cr, Mn, Fe, Co, Ni, Cu and Zn. The trivalent elements were selected from Ti, V, Cr, Mn, Fe, Co, Ni and Cu. These metals excluding Mg were chosen from period 4 elements. Crystal structures used for examination of phase relationships were extracted from the inorganic crystal structure database (ICSD). The selected structures were only ordered structures. Initial structures for first principle calculations were made from the extracted crystal structures. The extracted crystal structures were substituted the original metal element with each selected element. The extracted structures and substituted structures were calculated by first principle calculations. Tables 1.1 to 1.4 show the extracted crystal structures from the ICSD. These tables listed composition, structure type, space group and prototype. The prototype

means initial composition contained in the ICSD.

Formation energies in pseudo-ternary systems were calculated by first principle calculations. The Gibbs free energy is expressed as below.

$$G = H - TS \quad (3)$$

$$H = E + PV \quad (4)$$

$$G = E + PV - TS \quad (5)$$

G is the Gibbs free energy of the system. T is the temperature of the system. S is the entropy of the system. H is the enthalpy of the system. E is the internal energy of the system. P is the pressure of the system. V is the volume of the system. In the present systems, differences in PV term are negligible. Furthermore internal energies calculated by first principle calculations are at 0K. Therefore formation energies were calculated from internal energies.

All internal energy were calculated by density functional theory (DFT) using a generalized gradient approximation (GGA) functional parameterized by Perdew, Burke and Ernzerhof (PBE) [33]. All calculations were performed by Vienna ab initio simulation package (VASP) [34] with the projector augmented-wave (PAW) [35] potentials. The plane wave cutoff energy was set at 500eV. Almost all calculations were used with spin polarization and Hubbard U parameters for some transition metals. The calculations contained magnesium and zinc were not used with Hubbard U parameters. All magnetic moments of transition

metals were set initial state to high spin. We used two *U* parameters. One *U* parameter for Ti, V and Cr was 2eV and the other *U* parameter for Mn, Fe, Co, Ni and Cu was 4eV [36-39]. The *k* mesh was sampled according to a Monkhorst-Pack scheme [40] with a spacing of 0.5 /Å.

Thermodynamic stabilities of all compounds within the corresponding pseudo-ternary systems were examined in the following way. Firstly formation energies of all compounds within the corresponding pseudo-ternary systems were plotted with reference to the energy of three end-member compounds in the diagram. Then the convex hull of the formation energy was made. When a compound was located on the hull, the compound was regarded as “thermodynamically stable”. All of such thermodynamically stable compounds are shown as the apex of triangles in the diagram. As will be shown in Figures 1-1 to 1-9, all apexes was shown by orange closed circles and was connected by lines to form triangles. Orange closed circles will be called “negative formation energy”. When the formation energy of a compound was higher than the convex hull, the compound was regarded as “thermodynamically unstable”. They will be shown either by light-blue or dark-blue closed circles depending upon the magnitude of the formation energy. Light-blue closed circles corresponded to the formation energies between 0 to 0.1eV/cation, which will be called “slightly positive formation energy”. Dark-blue closed circles correspond to the formation energies > 0.1eV/cation, which will be called “highly positive formation

energy”.

Table 1.1 Crystal structures extracted from the ICSD

Composition	Structure type	Space group	Prototype
Li_2O		*R*-3*m*	Li_2O
P_2O_5	P_2O_5	*R*3*c*	P_2O_5
	P_2O_5(oP28)	*Pnma*	P_2O_5
$LiPO_3$		*Pc*	$LiPO_3$
		$P2_1/c$	$Li_6(P_6O_{18})$
Li_3PO_4	Cu_3AsS_4	$Pmn2_1$	$Li_3(PO_4)$
$Li_4P_2O_7$		$P2_1/c$	$Li_4(P_2O_7)$
		P-1	$Li_4(P_2O_7)$
		P-1	$Li_4(P_2O_7)$
MO	NaCl	*Fm*-3*m*	FeO
	CuO(mS8)	*C*2/*c*	CuO
	ZnS(2H)	$P6_3mc$	CoO
	ZnS(cF8)	*F*-43*m*	CoO
	CaO(hP4)	$P6_3mc$	MgO
	CsCl	*Pm*-3*m*	ZnO
	NiAs	$P6_3mc$	ZnO
		*P*3	MgO
		*C*2/*m*	TiO
M_2O_3	Al_2O_3	*R*-3*c*	Fe_2O_3
	V_2O_3	*C*2/*c*	V_2O_3
	Mn_2O_3	*Ia*-3	Fe_2O_3
	Mn_2O_3-alpha	*Pbca*	Mn_2O_3
	Sm_2O_3(cI80)	$I2_13$	Mn_2O_3
	$AlFeO_3$	$Pna2_1$	Fe_2O_3
		*P*3	Fe_2O_3
	Rh_2S_3	*Pbcn*	Fe_2O_3

Table 1.2 Crystal structures extracted from the ICSD

Composition	Structure type	Space group	Prototype
Li_6MO_4	Li_6ZnO_4	$P4_2/nmc$	$Li_6(CoO_4)$
$Li_{10}M_4O_9$		$P4_2/nmc$	$Li_{10}(Zn_4O_9)$
Li_2MO_2	La_2O_3	$P\text{-}3m1$	Li_2MnO_2
	Li_2CuO_2	$Immm$	Li_2CuO_2
		$C2/m$	Li_2CuO_2
Li_5MO_4	Li_5GaO_4-alpha	$Pbca$	Li_5FeO_4
Li_3MO_3	Au_4KSn_2	$P4_2/mnm$	Li_3CuO_3
$LiMO_2$	$LiFeO_2$-alpha	$I4_1/amd$	$LiFeO_2$
	$LiTiO_2$	$Fd\text{-}3m$	$LiTiO_2$
	$NaCrS_2$	$R\text{-}3m$	$LiFeO_2$
	$NaNiO_2$(mS8)	$C2/m$	$LiCuO_2$
		$Pmm2$	$LiMnO_2$
LiM_5O_8	$LiFe_5O_8$	$P4_332$	$Fe((Li_{0.5}Fe_{1.5})O_4$
MP_4O_{11}	MnP_4O_{11}	$P\text{-}1$	$Fe(P_4O_{11})$
	MgP_4O_{11}	$P2_1/c$	$Mg(P_4O_{11})$
		$P2_1/c$	$Mn(P_4O_{11})$
		$P2_1/c$	$Ni(P_4O_{11})$
$M(PO_3)_2$	$Ni_2(PO_3)_4$	$C2/c$	$Fe(P_4O_{12})$
	$ThTi_2O_6$(mS36)	$C2/c$	$Zn(PO_3)_2$
		Cc	$Zn(PO_3)_2$
$M_2P_2O_7$	$Fe_2P_2O_7$	$P1$	$Fe_2(P_2O_7)$
	$Y_2Si_2O_7$	$P2_1/c$	$Fe_2P_2O_7$
	$Co_2P_2O_7$	$P2_1/c$	$Co_2(P_2O_7)$
	$Sc_2Si_2O_7$	$C2/c$	$Mn_2P_2O_7$
	$Cu_2P_2O_7$	$C2/c$	$Cu_2(P_2O_7)$
	$Zn_2P_2O_7$	$C2/c$	$Zn_2(P_2O_7)$
		$Pbcm$	$Zn_2(P_2O_7)$

Table 1.3 Crystal structures extracted from the ICSD

Composition	Structure type	Space group	Prototype
$M_3(PO_4)_2$	$Fe_3(PO_4)_2$(mP52)	$P2_1/c$	$Fe_3(PO_4)_2$
	$Fe_3(PO_4)_2$(mP26)	$P2_1/c$	$Co_3(PO_4)_2$
	$Mg_3(PO_4)_2$	$P2_1/c$	$Co_3(PO_4)_2$
		$P2_1/c$	$Zn_3(PO_4)_2$
		$P2_1/c$	$Mn_3(PO_4)_2$
	$Mg_3(PO_4)_2$(P1-)	P-1	$Mg_3(PO_4)_2$
	$Cu_3(PO_4)_2$(P1-)	P-1	$Cu_3(PO_4)_2$
$M_4(PO_4)_2O$		$P2_1/c$	$Fe_4(PO_4)_2O$
		P-1	$Cu_4O(PO_4)_2$
	$Cu_4(PO_4)_2O$	$Pnma$	$Cu_4O(PO_4)_2$
$M_5O_2(PO_4)_2$		P-1	$Cu_5O_2(PO_4)_2$
$M(P\ O_3)_3$	$Rh(PO_3)_3$	Cc	$Fe(PO_3)_3$
	$V(PO_3)_3$	Cc	$V(PO_3)_3$
		$Pccn$	$Mn(P_3O_9)$
		$P2_1/c$	$Cr_2(P_6O_{18})$
		$C2/c$	$Cr(PO_3)_3$
$M_2P_4O_{13}$		$P2_1/c$	$Cr_2P_4O_{13}$
$M_4(P_2O_7)_3$		$P2_1/c$	$Fe_4(P_2O_7)_3$
		$Pnma$	$V_4(P_2O_7)_3$
MPO_4	$AlPO_4$	$P3_121$	$Fe(PO_4)$
	$AlPO_4$(HT)	$P6_422$	$Fe(PO_4)$
	$FePO_4$	$Pnma$	$Fe(PO_4)$
		$Pbca$	$Fe(PO_4)$
	$CrVO_4$	$Cmcm$	$Fe(PO_4)$
		$P2_1/c$	$Ti(PO_4)$
		$P2_1/c$	$Fe(PO_4)$
		$Imma$	$CrPO_4$

Table 1.4 Crystal structures extracted from the ICSD

Composition	Structure type	Space group	Prototype
$M_3(PO_4)O_3$	$Fe_3PO_4O_3$	*R*3*m*	$Fe_3(PO_4)O_3$
$LiM_2P_3O_{10}$	$LiCo_2P_3O_{10}$	$P2_1/c$	$LiCo_2(P_3O_{10})$
$LiMP_3O_9$	$CuLiP_3O_9$	$P2_12_12_1$	$LiFeP_3O_9$
		P-1	$Cu_2Li_2P_6O_{18}$
$Li_2M_3(P_2O_7)_2$		$P2_1/c$	$Li_2Ni_3(P_2O_7)_2$
$LiMPO_4$	Mg_2SiO_4	*Pnma*	$LiFe(PO_4)$
	Na_2CrO_4	*Cmcm*	$LiFe(PO_4)$
		$Pna2_1$	$LiZn(PO_4)$
	$LiGaSiO_4$	*R*3	$LiZn(PO_4)$
$Li_2MP_2O_7$		$P2_1/c$	$Li_2Mn(P_2O_7)$
	$Na_2PdP_2O_7$	*C*2/*c*	$Li_2Cu(P_2O_7)$
$Li_4M(PO_4)_2$		$P2_1/c$	$Li_4Zn(PO_4)_2$
$Li_9M_3(P_2O_7)_3(PO_4)_2$	$Li_9Al_3(P_2O_7)_3(PO_4)_2$	*P*-3*c*1	$Li_9Fe_3(P_2O_7)_3(PO_4)_2$
$LiMP_2O_7$	$LiInP_2O_7$	$P2_1$	$LiFe(P_2O_7)$
$Li_3M_2(PO_4)_3$	$Li_3Fe_2(PO_4)_3$	$P2_1/c$	$Li_3Fe_2(PO_4)_3$
	$Li_3In_2(PO_4)_3$	*R*-3	$Li_3Fe_2(PO_4)_3$

2-3 Results and Discussion

The phase relationships in pseudo-ternary systems of $1/2Li_2O$-MO-$1/2P_2O_5$ and $1/2Li_2O$-$1/2M_2O_3$-$1/2P_2O_5$ were examined by first principle calculations. The number of compounds calculated by first principle calculations was 796. The number of compounds contained in the ICSD was 164. The numbers of compositions in pseudo-ternary system of $1/2Li_2O$-MO-$1/2P_2O_5$ and $1/2Li_2O$-$1/2M_2O_3$-$1/2P_2O_5$ were 18 and 15, respectively.

2-3-1 $1/2Li_2O$-TiO-$1/2P_2O_5$ and $1/2Li_2O$-$1/2Ti_2O_3$-$1/2P_2O_5$ systems

Figure 1.1 (a) shows the phase relationship in pseudo-ternary system of $1/2Li_2O$-TiO-$1/2P_2O_5$. The numbers of apexes belonging to “negative formation energy”, “slightly positive formation energy” and “highly positive formation energy” were 9, 4 and 5, respectively. On the other hand, the ICSD did not contain lithium titanium(II) oxides, titanium(II) phosphates and lithium titanium(II) phosphates.

Figure 1.1 (b) shows the phase relationship in pseudo-ternary system of $1/2Li_2O$-$1/2Ti_2O_3$-$1/2P_2O_5$. The numbers of apexes belonging to “negative formation energy”, “slightly positive formation energy” and “highly positive formation energy” were 8, 5 and 2, respectively. On the other hand, the calculated compounds given in the ICSD were 6. Compositions of these compounds were $LiTiO_2$, $Ti(PO_3)_3$, $TiPO_4$ and $LiTiP_2O_7$. These compounds belonged to “negative formation energy” or

"slightly positive formation energy". $LiTiO_2$, $TiPO_4$ and $LiTiP_2O_7$ had negative formation energies. The stoichiometric compound of $Li_3Ti_2(PO_4)_3$ was not contained in the ICSD but nonstoichiometric compound with a Nasicon-type structure is obtained by the chemical lithiation of $LiTi_2(PO_4)_3$ [41]. This compound also belongs to "negative formation energy".

2-3-2 $1/2Li_2O$-VO-$1/2P_2O_5$ and $1/2Li_2O$-$1/2V_2O_3$-$1/2P_2O_5$ systems

Figure 1.2 (a) shows the phase relationship in pseudo-ternary system of $1/2Li_2O$-VO-$1/2P_2O_5$. The numbers of apexes belonging to "negative formation energy", "slightly positive formation energy" and "highly positive formation energy" were 10, 5 and 3, respectively. On the other hand, the ICSD did not contain lithium vanadium(II) oxides, vanadium(II) phosphates and lithium vanadium(II) phosphates.

Figure 1.2 (b) shows the phase relationship in pseudo-ternary system of $1/2Li_2O$-$1/2V_2O_3$-$1/2P_2O_5$. The numbers of apexes belonging to "negative formation energy", "slightly positive formation energy" and "highly positive formation energy" were 8, 6 and 1, respectively. On the other hand, the calculated compounds given in the ICSD were 8. Compositions of these compounds were $LiVO_2$, $V(PO_3)_3$, $V_4(P_2O_7)_3$, VPO_4, $Li_5(VO)(PO_4)_2$, $LiVP_2O_7$ and $Li_3V_2(PO_4)_3$. These compounds belonged to "negative formation energy" or "slightly positive formation energy". $LiVO_2$, $LiVP_2O_7$ and $Li_3V_2(PO_4)_3$ had negative formation

energies.

2-3-3 $1/2Li_2O$-CrO-$1/2P_2O_5$ and $1/2Li_2O$-$1/2Cr_2O_3$-$1/2P_2O_5$ systems

Figure 1.3 (a) shows the phase relationship in pseudo-ternary system of $1/2Li_2O$-CrO-$1/2P_2O_5$. The numbers of apexes belonging to “negative formation energy”, “slightly positive formation energy” and “highly positive formation energy” were 9, 7 and 2, respectively. On the other hand, the calculated compounds given in the ICSD were 2. Compositions of these compounds were $Cr_2P_2O_7$ and $Cr_3(PO_4)_2$. These compounds belonged to “slightly positive formation energy”. The formation energies of $Cr_2P_2O_7$ and $Cr_3(PO_4)_2$ were between 0 to 0.1eV/cation.

Figure 1.3 (b) shows the phase relationship in pseudo-ternary system of $1/2Li_2O$-$1/2Cr_2O_3$-$1/2P_2O_5$. The numbers of apexes belonging to “negative formation energy”, “slightly positive formation energy” and “highly positive formation energy” were 9, 2 and 4, respectively. On the other hand, the calculated compounds given in the ICSD were 9. Compositions of these compounds were $LiCrO_2$, $Cr(PO_3)_3$, $Cr_2P_4O_{13}$, $CrPO_4$, $Li_9Cr_3(P_2O_7)_3(PO_4)_2$, and $LiCrP_2O_7$. These compounds belonged to “negative formation energy” or “slightly positive formation energy”. $Cr(PO_3)_3$, $CrPO_4$, $Li_9Cr_3(P_2O_7)_3(PO_4)_2$, and $LiCrP_2O_7$ had negative formation energies.

2-3-4 $1/2Li_2O$-MnO-$1/2P_2O_5$ and $1/2Li_2O$-$1/2Mn_2O_3$-$1/2P_2O_5$ systems

Figure 1.4 (a) shows the phase relationship in pseudo-ternary system of $1/2Li_2O$-MnO-$1/2P_2O_5$. The numbers of apexes belonging to "negative formation energy", "slightly positive formation energy" and "highly positive formation energy" were 10, 5 and 3, respectively. On the other hand, the calculated compounds given in the ICSD were 10. Compositions of these compounds were Li_2MnO_2, MnP_4O_{11}, $Mn(PO_3)_2$, $Mn_2P_2O_7$, $Mn_3(PO_4)_2$, $LiMnP_3O_9$, $LiMnPO_4$ and $Li_2MnP_2O_7$. These compounds belonged to "negative formation energy" or "slightly positive formation energy". MnP_4O_{11}, $Mn(PO_3)_2$ and $LiMnPO_4$ had negative formation energies.

Figure 1.4 (b) shows the phase relationship in pseudo-ternary system of $1/2Li_2O$-$1/2Mn_2O_3$-$1/2P_2O_5$. The numbers of apexes belonging to "negative formation energy", "slightly positive formation energy" and "highly positive formation energy" were 7, 7 and 1, respectively. On the other hand, the calculated compounds given in the ICSD were 5. Compositions of these compounds were $LiMnO_2$, $Mn(PO_3)_3$, $MnPO_4$ and $LiMnP_2O_7$. These compounds belonged to "negative formation energy" or "slightly positive formation energy". $MnPO_4$ and $LiMnP_2O_7$ had negative formation energies.

2-3-5 $1/2Li_2O$-FeO-$1/2P_2O_5$ and $1/2Li_2O$-$1/2Fe_2O_3$-$1/2P_2O_5$ systems

Figure 1.5 (a) shows the phase relationship in pseudo-ternary system

of $1/2Li_2O$-FeO-$1/2P_2O_5$. The numbers of apexes belonging to “negative formation energy”, “slightly positive formation energy” and “highly positive formation energy” were 11, 7 and 0, respectively. On the other hand, the calculated compounds given in the ICSD were 10. Compositions of these compounds were FeP_4O_{11}, $Fe(PO_3)_2$, $Fe_2P_2O_7$, $Fe_3(PO_4)_2$, $Fe_4(PO_4)_2$, $LiFeP_3O_9$, $Li_2Fe_3(PO_4)_2$ and $LiFePO_4$. These compounds belonged to “negative formation energy” or “slightly positive formation energy”. $Fe(PO_3)_2$, $Fe_3(PO_4)_2$, $Fe_4(PO_4)_2$, and $LiFePO_4$ had negative formation energies.

Figure 1.5 (b) shows the phase relationship in pseudo-ternary system of $1/2Li_2O$-$1/2Fe_2O_3$-$1/2P_2O_5$. The numbers of apexes belonging to “negative formation energy”, “slightly positive formation energy” and “highly positive formation energy” were 9, 6 and 0, respectively. On the other hand, the calculated compounds given in the ICSD were 17. Compositions of these compounds were Li_5FeO_4, $LiFeO_2$, $LiFe_5O_8$, $Fe(PO_3)_3$, $Fe_4(P_2O_7)_3$, $FePO_4$, $Fe_3(PO_4)O_3$, $Li_9Fe_3(P_2O_7)_3(PO_4)_2$, $LiFeP_2O_7$ and $Li_3Fe_2(PO_4)_3$. These compounds belonged to “negative formation energy” or “slightly positive formation energy”. Li_5FeO_4, $LiFeO_2$, $FePO_4$, $LiFeP_2O_7$ and $Li_3Fe_2(PO_4)_3$ had negative formation energies.

2-3-6 $1/2Li_2O$-CoO-$1/2P_2O_5$ and $1/2Li_2O$-$1/2Co_2O_3$-$1/2P_2O_5$ systems

Figure 1.6 (a) shows the phase relationship in pseudo-ternary system

of $1/2Li_2O$-CoO-$1/2P_2O$. The numbers of apexes belonging to “negative formation energy”, “slightly positive formation energy” and “highly positive formation energy” were 10, 7 and 1, respectively. On the other hand, the calculated compounds given in the ICSD were 11. Compositions of these compounds were Li_6CoO_4, CoP_4O_{11}, $Co(PO_3)_2$, $Co_2P_2O_7$, $Co_3(PO_4)_2$, $LiCo_2P_3O_{10}$, $LiCoP_3O_9$ and $LiCoPO_4$. These compounds belonged to “negative formation energy” or “slightly positive formation energy”. Li_6CoO_4, $Co(PO_3)_2$, $Co_3(PO_4)_2$ and $LiCoP_3O_9$ had negative formation energies.

Figure 1.6 (b) shows the phase relationship in pseudo-ternary system of $1/2Li_2O$-$1/2Co_2O_3$-$1/2P_2O_5$. The numbers of apexes belonging to “negative formation energy”, “slightly positive formation energy” and “highly positive formation energy” were 9, 5 and 1, respectively. On the other hand, the calculated compounds given in the ICSD were 3. Compositions of these compounds were $LiCoO_2$ and $CoPO_4$. These compounds belonged to “negative formation energy”, “slightly positive formation energy” or “highly positive formation energy”. $LiCoO_2$ had negative formation energies.

2-3-7 $1/2Li_2O$-NiO-$1/2P_2O_5$ and $1/2Li_2O$-$1/2Ni_2O_3$-$1/2P_2O_5$ systems

Figure 1.7 (a) shows the phase relationship in pseudo-ternary system of $1/2Li_2O$-NiO-$1/2P_2O_5$. The numbers of apexes belonging to “negative formation energy”, “slightly positive formation energy” and “highly

positive formation energy" were 12, 3 and 3, respectively. On the other hand, the calculated compounds given in the ICSD were 12. Compositions of these compounds were Li_2NiO_2, NiP_4O_{11}, $Ni(PO_3)_2$, $Ni_2P_2O_7$, $Ni_3(PO_4)_2$, $LiNi_2P_3O_{10}$, $Li_2Ni_3(P_2O_7)_2$ and $LiNiPO_4$. These compounds belonged to "negative formation energy" or "slightly positive formation energy". Li_2NiO_2, NiP_4O_{11}, $Ni(PO_3)_2$, $Ni_3(PO_4)_2$, $LiNi_2P_3O_{10}$, $Li_2Ni_3(P_2O_7)_2$ and $LiNiPO_4$ had negative formation energies.

Figure 1.7 (b) shows the phase relationship in pseudo-ternary system of $1/2Li_2O$-$1/2Ni_2O_3$-$1/2P_2O_5$ The numbers of apexes belonging to "negative formation energy", "slightly positive formation energy" and "highly positive formation energy" were 7, 7 and 1, respectively.

On the other hand, the calculated compound given in the ICSD was 1. The composition of this compound was $LiNiO_2$. This compound belonged to "slightly positive formation energy".

2-3-8 $1/2Li_2O$-CuO-$1/2P_2O_5$ and $1/2Li_2O$-$1/2Cu_2O_3$-$1/2P_2O_5$ systems

Figure 1.8 (a) shows the phase relationship in pseudo-ternary system of $1/2Li_2O$-CuO-$1/2P_2O_5$. The numbers of apexes belonging to "negative formation energy", "slightly positive formation energy" and "highly positive formation energy" were 11, 6 and 1, respectively. On the other hand, the calculated compounds given in the ICSD were 13. Compositions of these compounds were Li_2CuO_2, CuP_4O_{11}, $Cu(PO_3)_2$, $Cu_2P_2O_7$, $Cu_3(PO_4)_2$, $LiCuP_3O_9$ and $Li_2CuP_2O_7$. These compounds

belonged to “negative formation energy” or “slightly positive formation energy”. Li_2CuO_2, CuP_4O_{11}, $Cu(PO_3)_2$, $Cu_3(PO_4)_2$, $LiCuP_3O_9$ and $Li_2CuP_2O_7$ had negative formation energies.

Figure 1.8 (b) shows the phase relationship in pseudo-ternary system of $1/2Li_2O$-$1/2Cu_2O_3$-$1/2P_2O_5$. The numbers of apexes belonging to “negative formation energy”, “slightly positive formation energy” and “highly positive formation energy” were 7, 3 and 5, respectively. On the other hand, the calculated compounds given in the ICSD were 2. Compositions of these compounds were $LiCuO_2$ and Li_3CuO_3. These compounds belonged to “negative formation energy”.

2-3-9 $1/2Li_2O$-ZnO-$1/2P_2O_5$ system

Figure 1.9 (a) shows the phase relationship in pseudo-ternary system of $1/2Li_2O$-ZnO-$1/2P_2O_5$. The numbers of apexes belonging to “negative formation energy”, “slightly positive formation energy” and “highly positive formation energy” were 10, 7 and 1, respectively.

On the other hand, the calculated compounds given in the ICSD were 13. Compositions of these compounds were Li_6ZnO_4, $Li_{10}Zn_4O_9$, ZnP_4O_{11}, $Zn(PO_3)_2$, $Zn_2P_2O_7$, $Zn_3(PO_4)_2$ and $LiZnPO_4$. These compounds belonged to “negative formation energy” or “slightly positive formation energy”. Li_6ZnO_4, $Li_{10}Zn_4O_9$, $Zn(PO_3)_2$, $Zn_2P_2O_7$, $Zn_3(PO_4)_2$, and $LiZnPO_4$ had negative formation energies.

2-3-10 $1/2Li_2O$-MgO-$1/2P_2O_5$ system

Figure 1.9 (b) shows the phase relationship in pseudo-ternary system of $1/2Li_2O$-MgO-$1/2P_2O_5$. The numbers of apexes belonging to “negative formation energy”, “slightly positive formation energy” and “highly positive formation energy” were 10, 7 and 1, respectively.

Figure 1.9 (a) shows the phase relationship in pseudo-ternary system of $1/2Li_2O$-ZnO-$1/2P_2O_5$. The numbers of apexes belonging to “negative formation energy”, “slightly positive formation energy” and “highly positive formation energy” were 10, 7 and 1, respectively. On the other hand, the calculated compounds given in the ICSD were 9. Compositions of these compounds were MgP_4O_{11}, $Mg(PO_3)_2$, $Mg_2P_2O_7$, $Mg_3(PO_4)_2$ and $LiMgPO_4$. These compounds belonged to “negative formation energy” or “slightly positive formation energy”. MgP_4O_{11}, $Mg(PO_3)_2$, $Mg_3(PO_4)_2$ and $LiMgPO_4$ had negative formation energies.

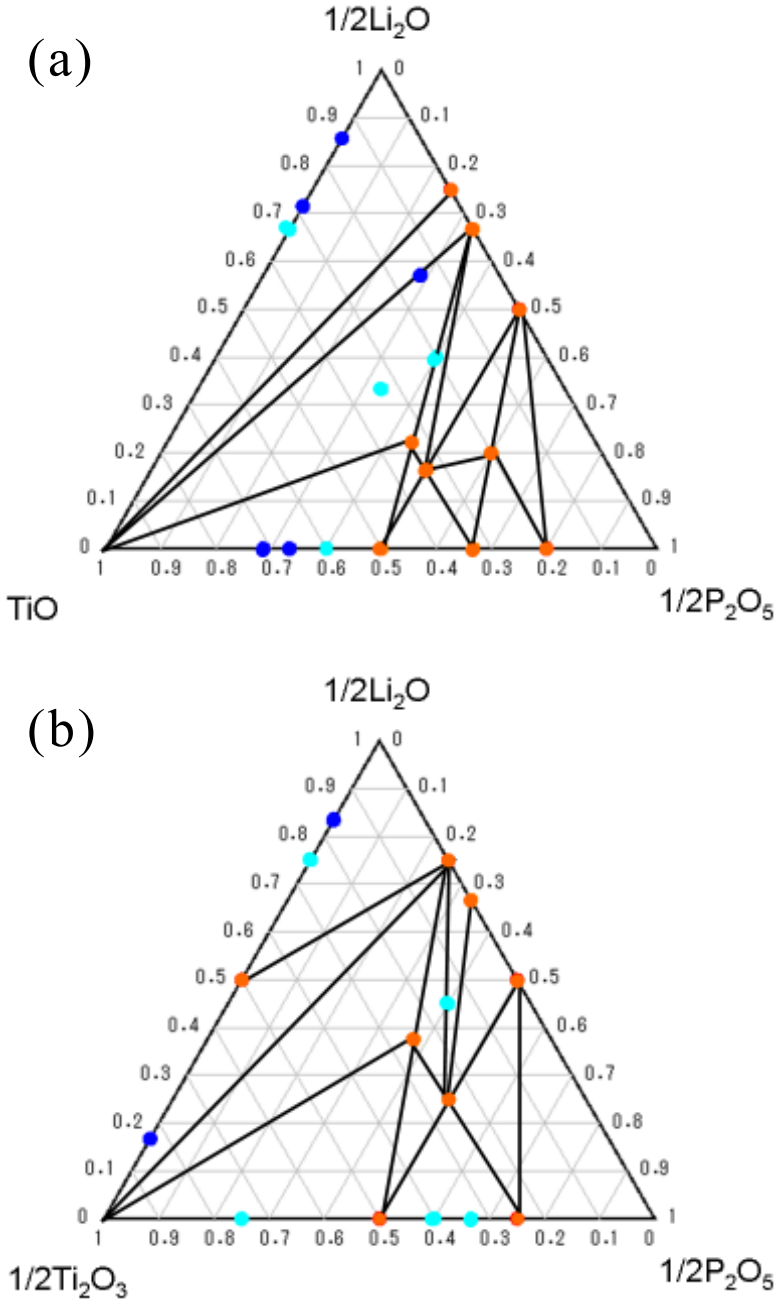

Figure 1.1 Phase relationships in pseudo-ternary systems of (a) $1/2Li_2O$-TiO-$1/2P_2O_5$ and (b) $1/2Li_2O$-$1/2Ti_2O_3$-$1/2P_2O_5$. Orange closed circles corresponded to the formation energies < 0eV/cation. Light-blue closed circles corresponded to the formation energies between 0 to 0.1eV/cation. Dark-blue closed circles corresponded to the formation energies > 0.1eV/cation.

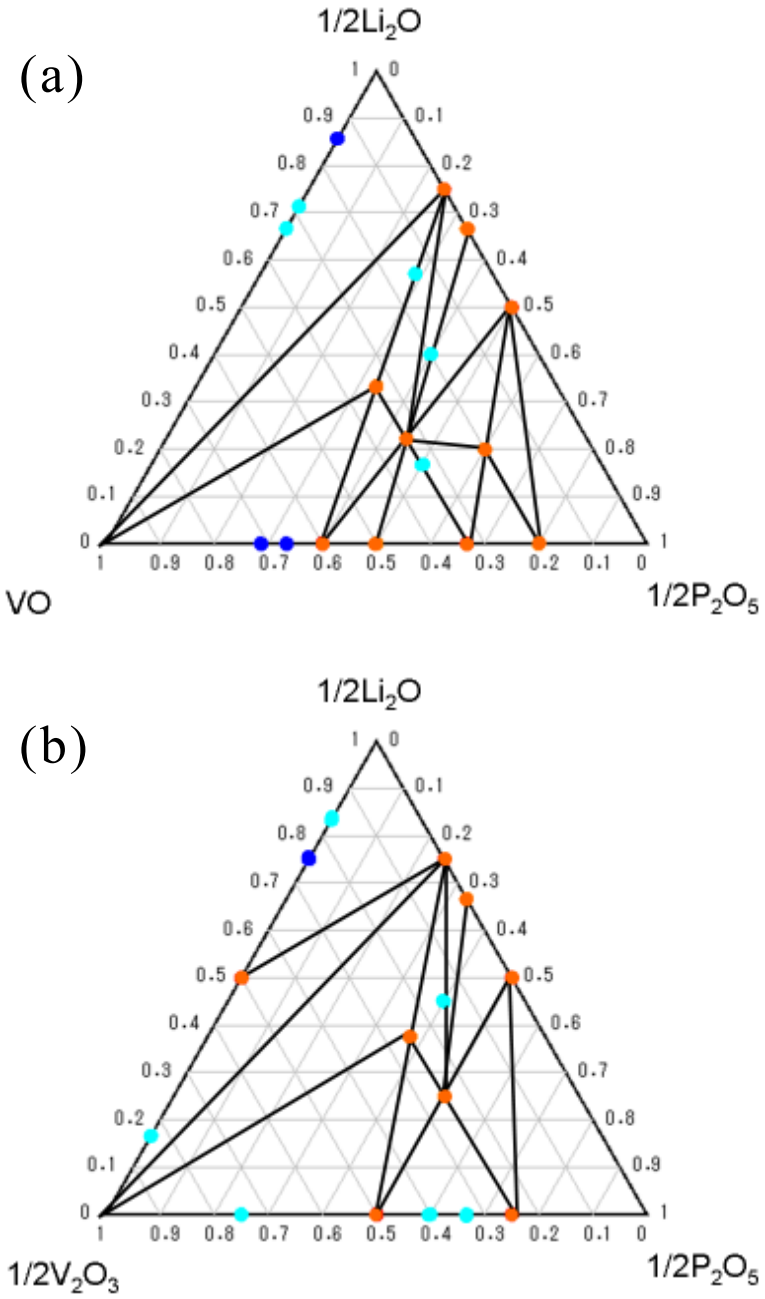

Figure 1.2 Phase relationships in pseudo-ternary systems of (a) $1/2Li_2O$-VO-$1/2P_2O_5$ and (b) $1/2Li_2O$-$1/2V_2O_3$-$1/2P_2O_5$. Orange closed circles corresponded to the formation energies < 0eV/cation. Light-blue closed circles corresponded to the formation energies between 0 to 0.1eV/cation. Dark-blue closed circles corresponded to the formation energies > 0.1eV/cation.

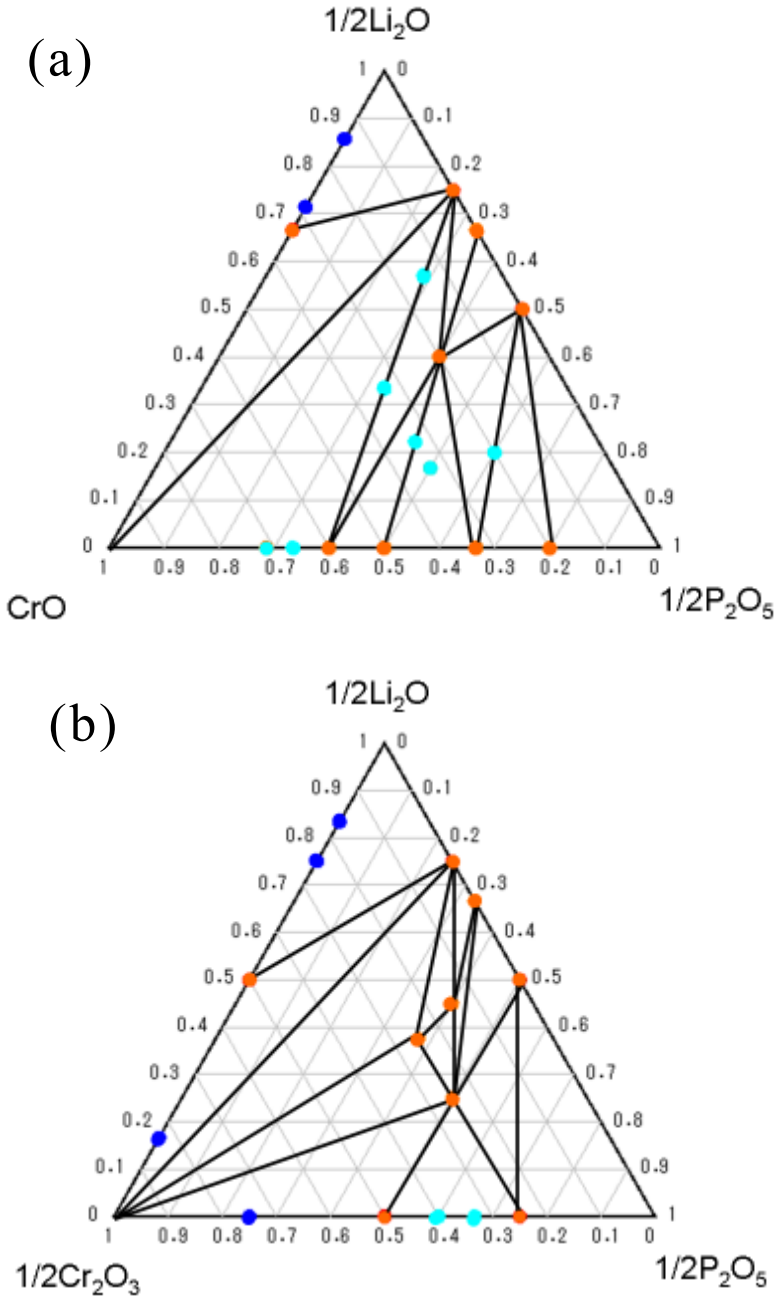

Figure 1.3 Phase relationships in pseudo-ternary systems of (a) $1/2Li_2O$-CrO-$1/2P_2O_5$ and (b) $1/2Li_2O$-$1/2Cr_2O_3$-$1/2P_2O_5$. Orange closed circles corresponded to the formation energies < 0eV/cation. Light-blue closed circles corresponded to the formation energies between 0 to 0.1eV/cation. Dark-blue closed circles corresponded to the formation energies > 0.1eV/cation.

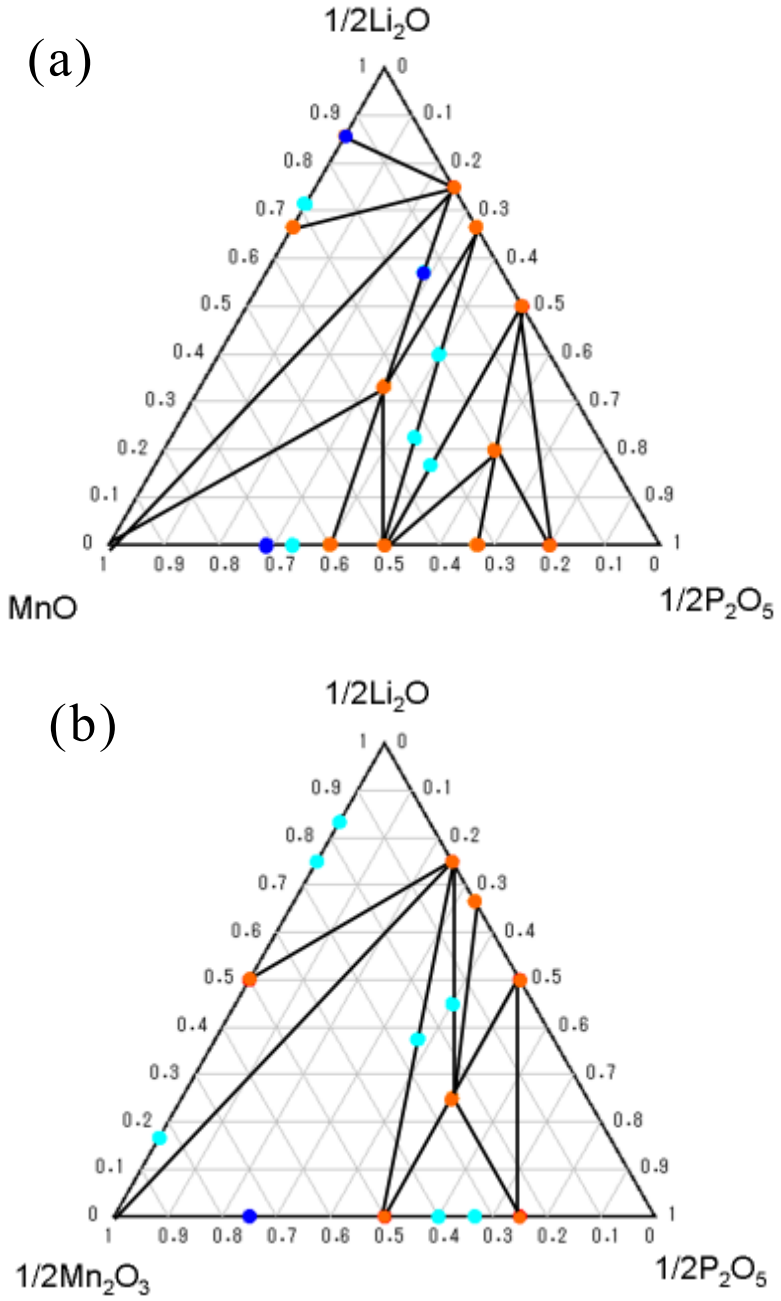

Figure 1.4 Phase relationships in pseudo-ternary systems of (a) $1/2Li_2O$-MnO-$1/2P_2O_5$ and (b) $1/2Li_2O$-$1/2Mn_2O_3$-$1/2P_2O_5$. Orange closed circles corresponded to the formation energies < 0eV/cation. Light-blue closed circles corresponded to the formation energies between 0 to 0.1eV/cation. Dark-blue closed circles corresponded to the formation energies > 0.1eV/cation.

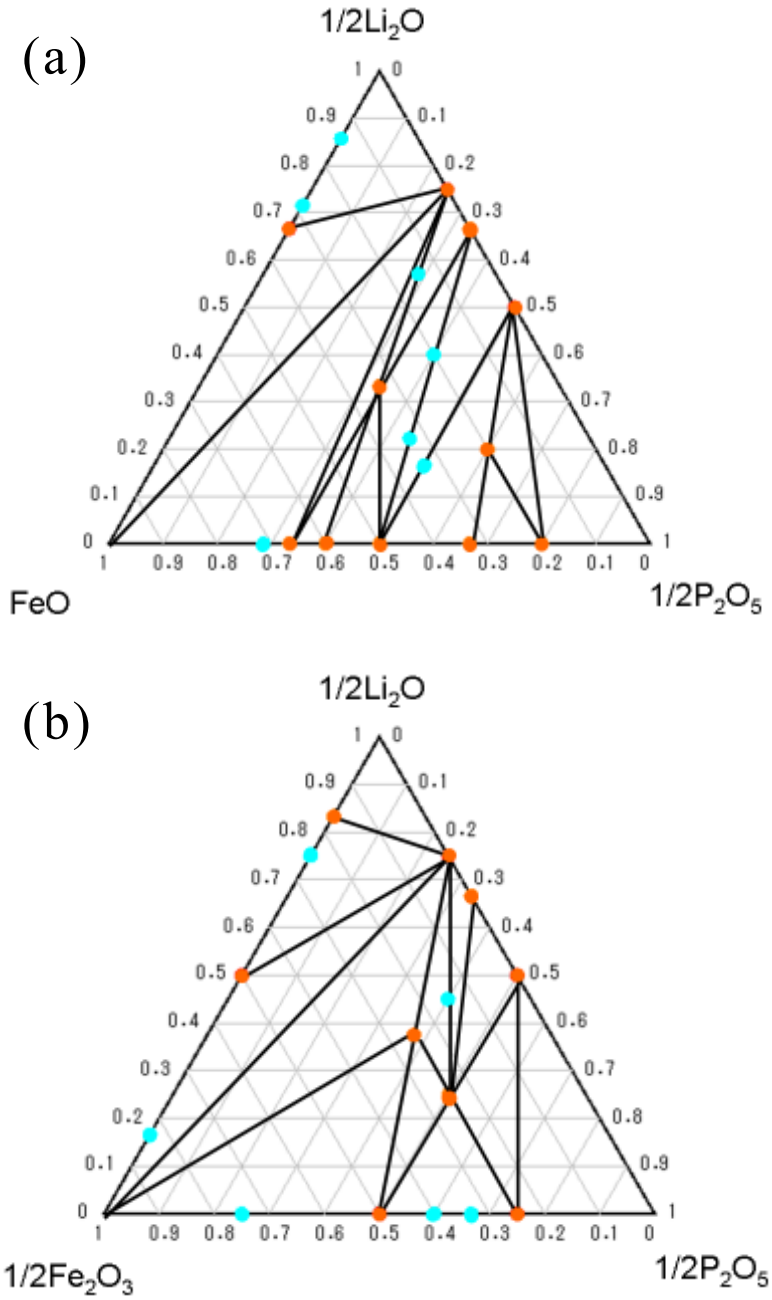

Figure 1.5 Phase relationships in pseudo-ternary systems of (a) $1/2Li_2O$-FeO-$1/2P_2O_5$ and (b) $1/2Li_2O$-$1/2Fe_2O_3$-$1/2P_2O_5$. Orange closed circles corresponded to the formation energies < 0eV/cation. Light-blue closed circles corresponded to the formation energies between 0 to 0.1eV/cation. Dark-blue closed circles corresponded to the formation energies > 0.1eV/cation.

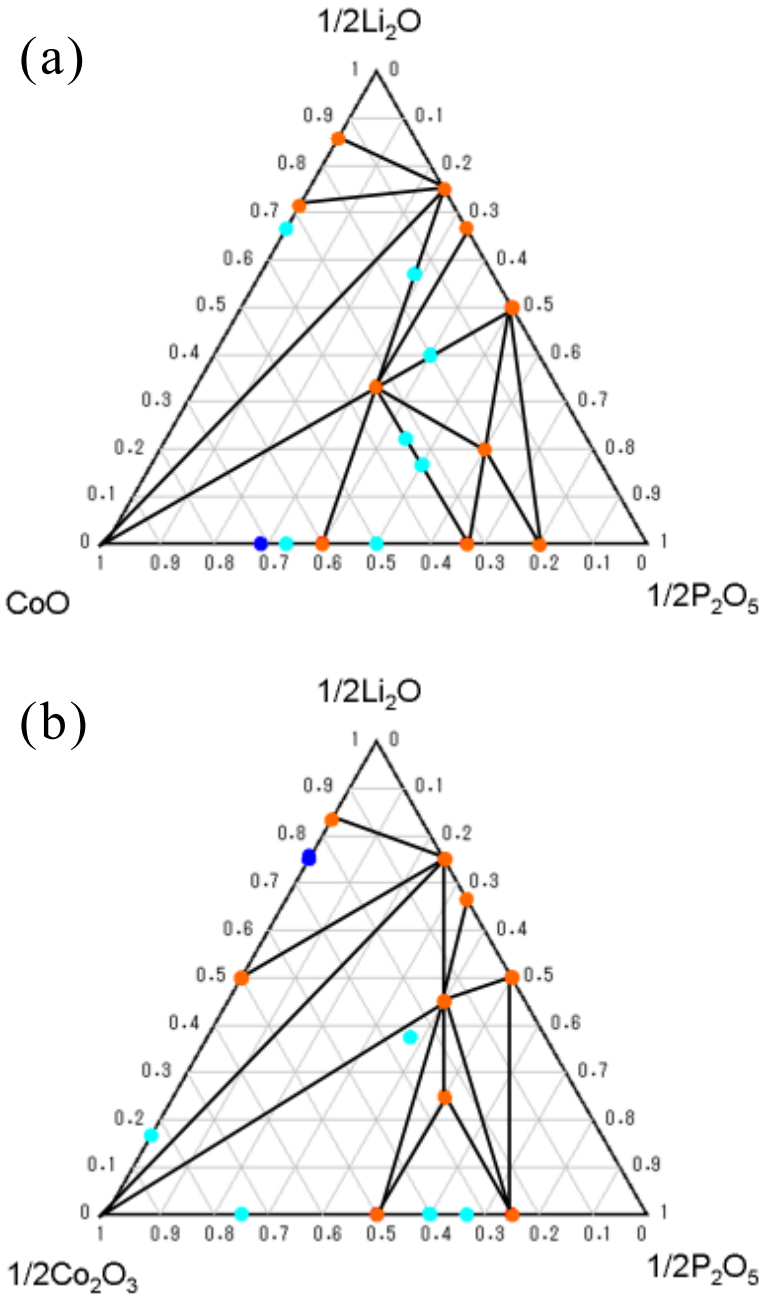

Figure 1.6 Phase relationships in pseudo-ternary systems of (a) $1/2Li_2O$-CoO-$1/2P_2O_5$ and (b) $1/2Li_2O$-$1/2Co_2O_3$-$1/2P_2O_5$. Orange closed circles corresponded to the formation energies < 0eV/cation. Light-blue closed circles corresponded to the formation energies between 0 to 0.1eV/cation. Dark-blue closed circles corresponded to the formation energies > 0.1eV/cation.

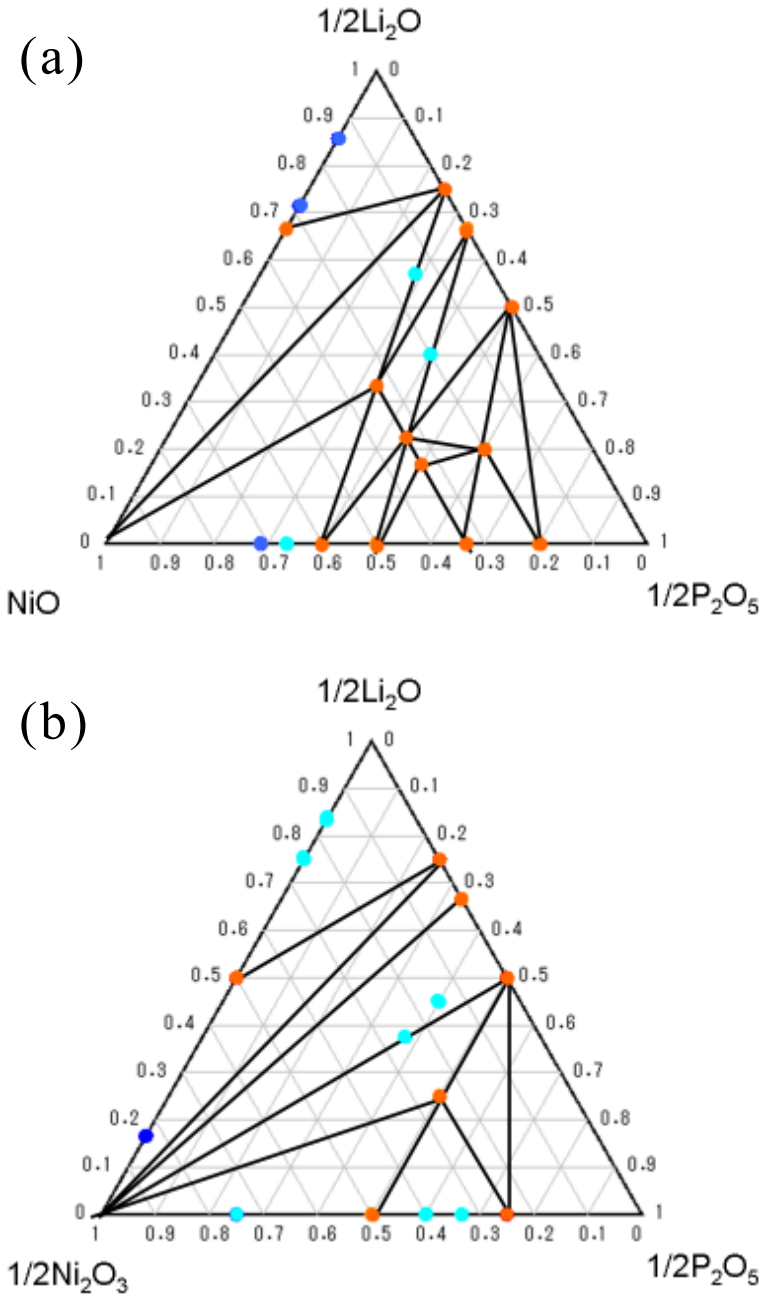

Figure 1.7 Phase relationships in pseudo-ternary systems of (a) $1/2Li_2O$-NiO-$1/2P_2O_5$ and (b) $1/2Li_2O$-$1/2Ni_2O_3$-$1/2P_2O_5$. Orange closed circles corresponded to the formation energies < 0eV/cation. Light-blue closed circles corresponded to the formation energies between 0 to 0.1eV/cation. Dark-blue closed circles corresponded to the formation energies > 0.1eV/cation.

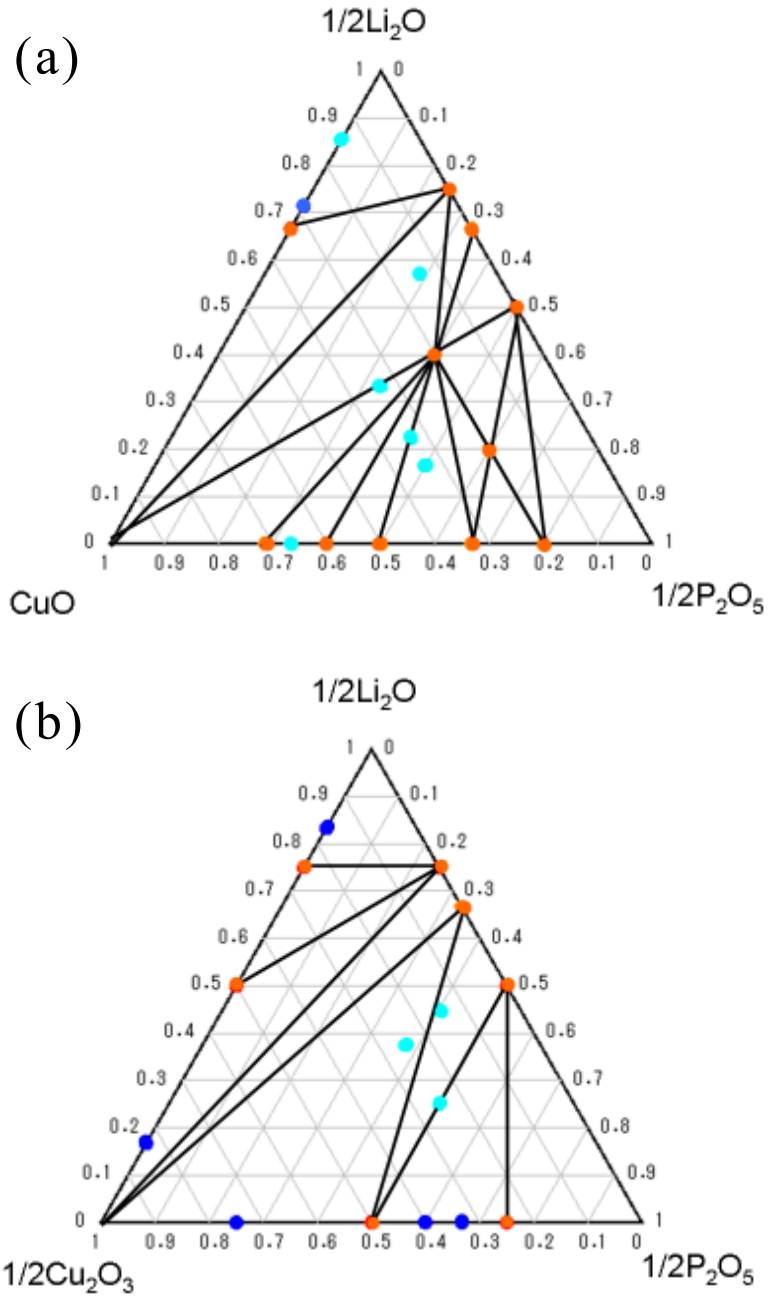

Figure 1.8 Phase relationships in pseudo-ternary systems of (a) $1/2Li_2O$-CuO-$1/2P_2O_5$ and (b) $1/2Li_2O$-$1/2Cu_2O_3$-$1/2P_2O_5$. Orange closed circles corresponded to the formation energies < 0eV/cation. Light-blue closed circles corresponded to the formation energies between 0 to 0.1eV/cation. Dark-blue closed circles corresponded to the formation energies > 0.1eV/cation.

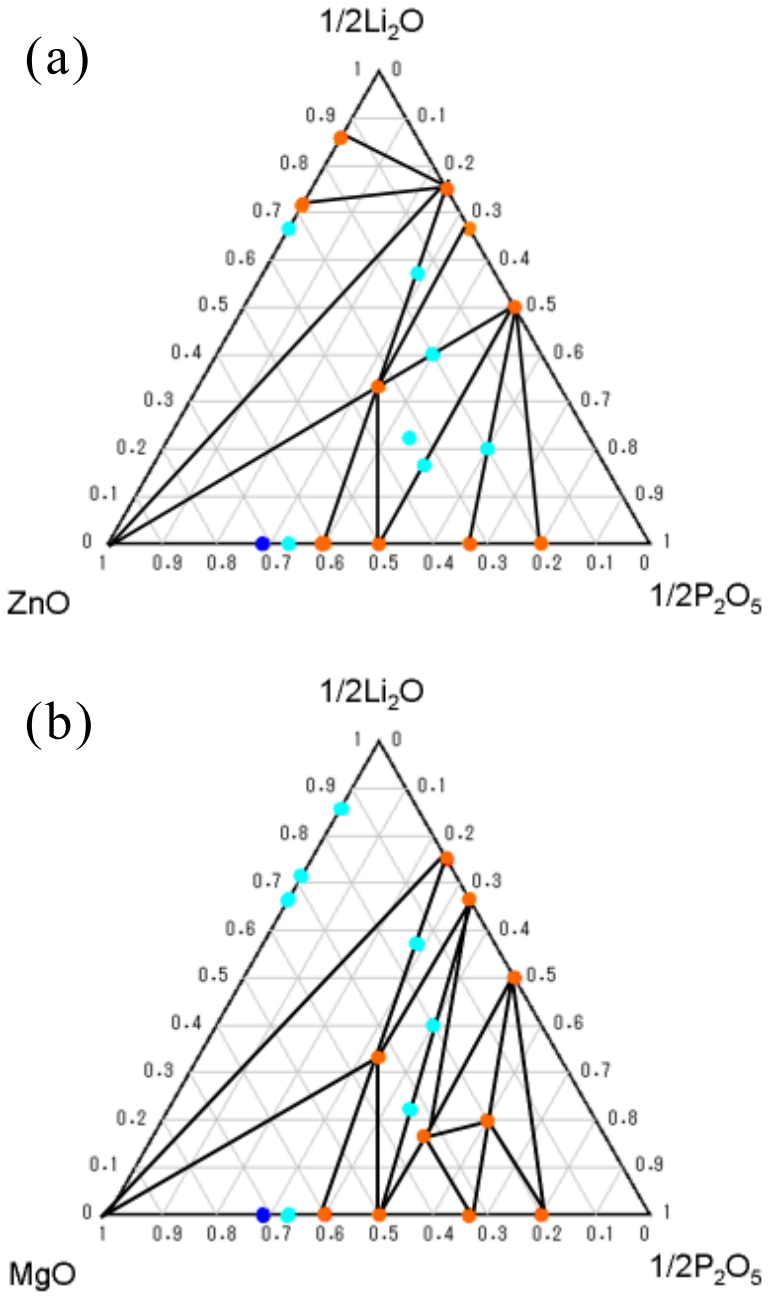

Figure 1.9 Phase relationships in pseudo-ternary systems of (a) $1/2Li_2O$-ZnO-$1/2P_2O_5$ and (b) $1/2Li_2O$-MgO-$1/2P_2O_5$. Orange closed circles corresponded to the formation energies < 0eV/cation. Light-blue closed circles corresponded to the formation energies between 0 to 0.1eV/cation. Dark-blue closed circles corresponded to the formation energies > 0.1eV/cation.

Figure 2 shows frequency distribution of a number of compounds on formation energies. The blue bar shows frequency distribution the number of all compounds calculated by first principle calculations. The red line shows frequency distribution the number of compounds given in the ICSD. The total number of all compounds calculated by first principle calculations was 796. The total number of calculated compounds given in the ICSD was 164.

The number of compounds with negative formation energy was 63 in calculated compounds given in the ICSD. This result indicates that 62% of calculated compounds given in the ICSD were thermodynamically unstable. Nevertheless, these materials were synthesized. Much of the phosphate materials formed thermodynamically unstable structures.

The number of compounds with negative formation energy was 132 in all calculated compounds. The majority of compounds were distributed the formation energy with 0 to 0.1eV/cation. If some compounds have not been attempted synthesis, these compounds might contain a new material.

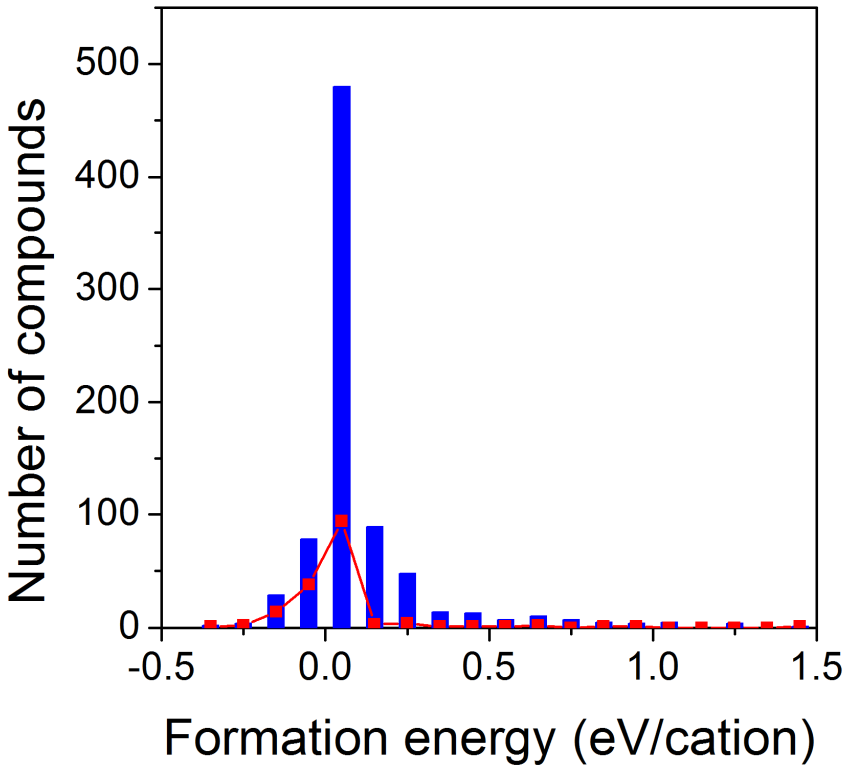

Figure 2 Frequency distribution of a number of compounds on formation energies. The blue bar shows frequency distribution the number of all compounds calculated by first principle calculations. The red line shows frequency distribution the number of compounds given in the ICSD.

2-4 Summary

1. The phase relationships in pseudo-ternary systems of $1/2Li_2O$-MO-$1/2P_2O_5$ and $1/2Li_2O$-$1/2M_2O_3$-$1/2P_2O_5$ were examined by first principle calculations (Figure 1.1 to Figure 1.9).
2. The formation energy was calculated at each compound. All apexes were classified into three groups, namely “negative formation energy”, “slightly positive formation energy” and “highly positive formation energy”.
3. The total number of all compounds calculated by first principle calculations was 796. The total number of calculated compounds given in the ICSD was 164.
4. The number of compounds with negative formation energy was 63 in calculated compounds given in the ICSD. This result indicates that 62% of calculated compounds given in the ICSD were thermodynamically unstable. Much of the phosphate materials formed thermodynamically unstable structures.
5. The number of compounds with negative formation energy was only 132 in all calculated compounds. The majority of compounds were distributed the formation energy with 0 to 0.1eV/cation. If some compounds have not been attempted synthesis, these compounds might contain a new material.

References

[1] A.K.Padhi, K.S.Nanjundaswamy and J. B. Goodenough, Electrochem. Soc., 144(4), 1188-1194(1997)

[2] A.S. Andersson, J.O. Thomas, B. Kalska, L. Häggström, Electrochem. Solid-State Lett., 3, 66 (2000)

[3] N. Ravet, Y. Chouinard, J.F. Magnan, S. Besner, M. Gauthier, M. Armand, J. Power Sources, 97–98, 503-507 (2001)

[4] G. Li, H. Azuma and M. Tohda, Electrochem. Solid-State Lett., 5(6), A135-A137 (2002)

[5] K. Amine, H. Yasuda and M. Yamachi, Electrochem. Solid-State Lett., 3(4), 178-179 (2000)

[6] P. Barpanda, T. Ye, S. Chung, Y. Yamada, S. Nishimura and A. Yamada, J. Mater. Chem., 22, 13455 (2012)

[7] M. Y. Saı¨di, J. Barker, H. Huang, J. L. Swoyer and G. Adamson, Electrochem. Solid-State Lett., 5(7), A149-A151 (2002)

[8] Y. W. Xiao, J. Y. Lee, A. S. Yu and Z. L. Liu, J. Electrochem. Soc., 146(10), 3623-3629 (1999)

[9] H. Aono, E. Sugimoto, Y. Sadaoka, N. Imanaka and G. Adachi, J. Electrochem. Soc., 137(4), 1023-1027 (1990)

[10] A. S. Andersson,a, J. O. Thomas, B. Kalska and L. Häggströmb, Electrochem. Solid-State Lett., 3(2), 66-68 (2000)

[11] M. Takahashi, H. Ohtsuka, K. Akuto and Y. Sakurai, Electrochem. Soc., 152(5), A899-A904 (2005)

[12] D. Morgan, G. Ceder, M. Y. Saidi, J. Barker, J. Swoyer, H. Huang, G. Adamson, Chem. Mater., 14(11), 4684-4693 (2002).

[13] D. Morgan, G. Ceder, M. Y. Saidi, J. Barker, J. Swoyer, H. Huang and G. Adamson, J. Power Sources, 119, 755-759 (2003).

[14] D. Morgan, A. Van der Ven and G. Ceder, Electrochem. Solid State Lett., 7(2), A30-A32 (2004).

[15] F. Zhou, C.A. Marianetti, M. Cococcioni, D. Morgan and G. Ceder, Phys. Rev. B, 69, 201101 (2004)

[16] F. Zhou, K. Kang, T. Maxisch, G. Ceder and D. Morgan, Solid State Comm., 132, 181-186 (2004)

[17] T. Maxisch, F. Zhou and G. Ceder, Phys. Rev. B, 73, 104301 (2006)

[18] T. Maxisch and G. Ceder, Phys. Rev. B, 73, 174112 (2006)

[19] F. Zhou, T. Maxisch and G. Ceder, Phys. Rev. Lett., 97, 155704 (2006)

[20] L. Wang, F. Zhou, Y.S. Meng and G. Ceder, Phys. Rev. B, 76, 16435 (2007)

[21] S. P. Ong, L. Wang, B. Kang and G. Ceder, Chem. Mater., 20(5), 1798-1807 (2008)

[22] L. Wang, F. Zhou and G. Ceder, Electrochem. Solid-State Lett., 11(6), A94-A96 (2008)

[23] R. Malik, F. Zhou and G. Ceder, Phys. Rev. B, 79, 214201 (2009)

[24] S. P. Ong, A. Jain, G. Hautier, B. Kang and G. Ceder, Electrochem. Comm., 12(3), 427-430 (2010)

[25] S. P. Ong, V. L Chevrier and G. Ceder, Phys. Rev. B, 83(075112), 1-7 (2011)

[26] H. Zhou, S. Upreti, N.A. Chernova, G. Hautierand, G. Ceder,and M.S. Whittingham, Chem. Mater., 23(2), 293-300 (2011).

[27] A. Jain, G. Hautier, C. Moore, B. Kang, J. Lee, H. Chen, N. Twu and G. Ceder, J. Electrochem. Soc., 159(5), A622-A633 (2012).

[28] K. Rajan, Mater. Today, 8(10), 38-45 (2005)

[29] S. Curtarolo et al. Nature Mater., 12, 191–201(2013)

[30] G. Ceder, MRS BULLETIN, 35, (2010)

[31] G. Hautier, A. Jain, H. Chen, C. Moore, S. P. Ong and G. Ceder, J. Mater. Chem., 21, 17147-17153 (2011)

[32] R. Jalem, T. Aoyama, M. Nakayama and M. Nogami, Chem. Mater., 24, 1357−1364 (2012)

[33] J. P. Perdew, K. Burke and M. Ernzerhof, Phys. Rev. Lett., 77(18) 3865-3868 (1996)

[34] G. Kresse and J. Furthmuller, Phys. Rev. B, 54(16) 11169-11186 (1996)

[35] P. E. Blochl, Phys. Rev. B, 50(24) 17953-17979 (1994)

[36] V. I Anisimov, F Aryasetiawan and A I Lichtenstein, J. Phys.: Condens. Matter, 9, 767–808 (1997)

[37] V. I. Anisimov, J. Zaanen and O. K. Andersen, Phys. Rev. B, 44(3) 943-954 (1991)

[38] F. Zhou, M. Cococcioni, C. A. Marianetti, D. Morgan, and G. Ceder,

Phys. Rev. B, 70, 235121 (2004)

[39]W. Setyawan, R. M. Gaume, S. Lam, R. S. Feigelson and S. Curtarolo, ACS Comb. Sci., 13, 382–390 (2011)

[40] H. J. Monkhorst and J. D. Pack, Phys. Rev. B, 13, 5188 (1976)

[41] A. Aatiq, M. Me´ne´trier, L. Croguennec, E. Suard and C. Delmas, J. Mater. Chem., 12, 2971–2978 (2002)

Chapter 3
Comparative study of crystal structures of lithium metal phosphates

3-1 Introduction

Recently lithium-ion batteries have been used for not only portable devices but also large-scale electricity storages. Lithium-ion batteries have high-energy density, high-power density, low self-discharge and high efficiency between charge and discharge. The disadvantage of lithium-ion batteries is safety risk. Hence the component of lithium-ion batteries has been investigated. For example, $LiFePO_4$ is known to a stable cathode material [1-4] and $LiTi_2(PO_4)_3$ [5] is known to a solid state electrolyte. In this way, a phosphate material [6-8] is promising material for lithium-ion batteries.

Some of lithium metal phosphates were also studied by first principle calculations. The research group of Ceder calculated the materials for lithium-ion batteries by first principle calculations [9-24]. Furthermore some phase diagrams are now available on the open website of “Material Project”. These previous works attempted to shed light on a chemical

reaction and to explore a new material. Unfortunately, these calculations do not always guarantee that calculation results are consistent with experimental results. Therefore it was difficult to use for exploring new materials.

Materials informatics has been much attention in recent years [25-29]. The concept of materials informatics is to apply the principle of informatics to the material science. Materials informatics is the promising approach to discover a new material. Materials informatics needs a massive database and data mining technique. It believed that first principle calculations are contributed to make a massive database. However the adequacy of crystal structure data calculated by first principle calculation remains unclear.

In the present study, we performed the comparative study of crystal structures of lithium metal phosphates. This comparative study used not only thermodynamically stable structures but also thermodynamically unstable structures. The purpose of this study is to attempt the systematic survey in thermodynamically stable and unstable compounds.

3-2 Method

In this work, the basic data of crystal structure was investigated at pseudo-ternary systems. These pseudo-ternary systems are $1/2Li_2O$-MO-$1/2P_2O_5$ and $1/2Li_2O$-$1/2M_2O_3$-$1/2P_2O_5$. The divalent elements were selected from Mg, Ti, V, Cr, Mn, Fe, Co, Ni, Cu and Zn.

The trivalent elements were selected from Ti, V, Cr, Mn, Fe, Co, Ni and Cu. These metals excluding Mg were chosen from period 4 elements. Crystal structures used for examination of phase relationships were extracted from the inorganic crystal structure database (ICSD). Initial structures for first principle calculations were made from the extracted crystal structures. The extracted crystal structures were substituted the original metal element with each selected element. The extracted structures and substituted structures were calculated by first principle calculations. These calculated structures show Tables 1.1 to 1.4 in chapte2. Each phase relationship was examined by first principle calculations. These results show Figures 1.1 to 1.9 in chapter 2.

Formation energies of all compounds within the corresponding pseudo-ternary systems were plotted with reference to the energy of three end-member compounds in the diagram. Orange closed circles corresponded to the formation energies < 0eV/cation, which will be called “negative formation energy”. When the formation energy of a compound was higher than the convex hull, the compound was regarded as “thermodynamically unstable”. They will be shown either by light-blue or dark-blue closed circles depending upon the magnitude of the formation energy. Light-blue closed circles corresponded to the formation energies between 0 to 0.1eV/cation, which will be called “slightly positive formation energy”. Dark-blue closed circles correspond to the formation energies > 0.1eV/cation, which will be

called “highly positive formation energy”.

All internal energy were calculated by density functional theory (DFT) using a generalized gradient approximation (GGA) functional parameterized by Perdew, Burke and Ernzerhof (PBE) [30]. All calculations were performed by Vienna ab initio simulation package (VASP) [31] with the projector augmented-wave (PAW) [32] potentials. The plane wave cutoff energy was set at 500eV. Almost all calculations were used with spin polarization and Hubbard *U* parameters for some transition metals. The calculations contained magnesium and zinc were not used with Hubbard *U* parameters. All magnetic moments of transition metals were set initial state to high spin. We used two *U* parameters. One *U* parameter for Ti, V and Cr was 2eV and the other *U* parameter for Mn, Fe, Co, Ni and Cu was 4eV [33-36]. The *k* mesh was sampled according to a Monkhorst-Pack scheme [37] with a spacing of 0.5 /Å.

The coordination number of a central atom was counted as the number of oxygen atom. Each cation was used as the central atom and coordination number at each cation was counted. The number of oxygen atom was counted if the distance between cation and oxygen was less than 2.5Å. In crystal structure the bonds are not clearly defined. Hence the bonds were defined that distance between cation and oxygen was less than 2.5Å. According to Shannon crystal radii [38], oxygen ionic radius is about 1.26Å, so coordination number was counted if cation’s radius was less than 1.24Å.

3-3 Results and Discussion

Phase relationships in pseudo-ternary systems of $1/2Li_2O$-MO-$1/2P_2O_5$ and $1/2Li_2O$-$1/2M_2O_3$-$1/2P_2O_5$ were shown in chapter 2. The compounds calculated by first principle calculations were classified into three groups, namely “negative formation energy”, “slightly positive formation energy” and “highly positive formation energy”.

Figure 3.1 shows a number of divalent compounds with coordination numbers 4 and 6. Figure 3.2 shows a number of trivalent compounds with coordination numbers 4 and 6. The blue bar shows the number of compounds with coordination number 4 in compounds with negative formation energy. The red bar shows the number of compounds with coordination number 6 in compounds with negative formation energy. The blue line shows the number of compounds with coordination number 4 in all calculated compounds. The red line shows the number of compounds with coordination number 6 in all calculated compounds.

A number of divalent compounds were 50 and a number of trivalent compounds were 37. The initial structures had coordination numbers 3 to 8. The coordination number 3 was only one structure at each element and the coordination number 8 was also only one structure. The structures with coordination number 3 and 8 were thermodynamically unstable.

Figure 3.1 shows a number of divalent compounds with coordination numbers 4 and 6. All elements had compounds with coordination number 4 and 6. However some elements had only coordination number 6 in

compounds with negative formation energy. The chromium(II) compounds and copper(II) compounds with coordination number 4 were larger than coordination number 6 in all calculated compounds. The compounds of chromium(II), copper(II) and zinc(II) mainly had coordination number 4 in compounds with negative formation energy. On the other hand, the compounds of magnesium(II), titanium(II), vanadium(II) and manganese(II) had only coordination number 6 in compounds with negative formation energy. In the periodic table, elements of lower number group had coordination number 6 and elements of higher number group had coordination number 4.

Figure 3.2 shows a number of trivalent compounds with coordination numbers 4 and 6. All elements had compounds with coordination number 4 and 6. However some elements had only coordination number 6 in compounds with negative formation energy. The compounds of titanium(III), vanadium(III), chromium(III), manganese(III) and nickel(III) had only coordination number 6 in compounds with negative formation energy.

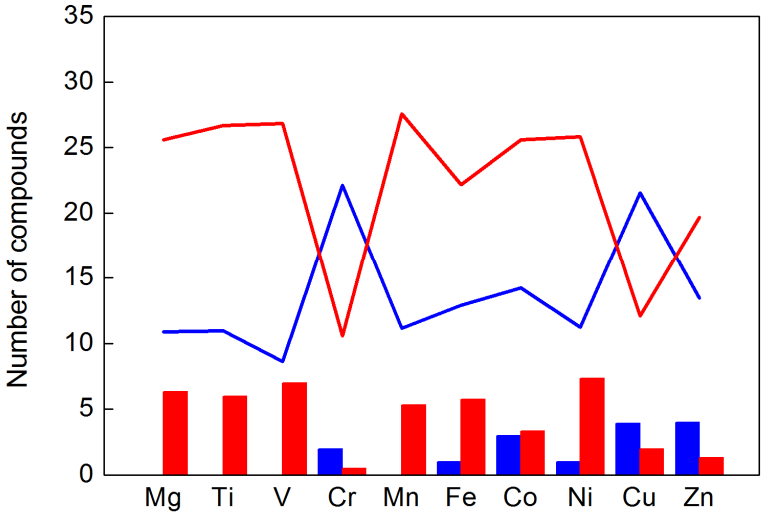

Figure 3.1 A number of divalent compounds with coordination numbers 4 and 6. The blue bar shows the number of compounds with coordination number 4 in compounds with negative formation energy. The red bar shows the number of compounds with coordination number 6 in compounds with negative formation energy. The blue line shows the number of compounds with coordination number 4 in all calculated compounds. The red line shows the number of compounds with coordination number 6 in all calculated compounds.

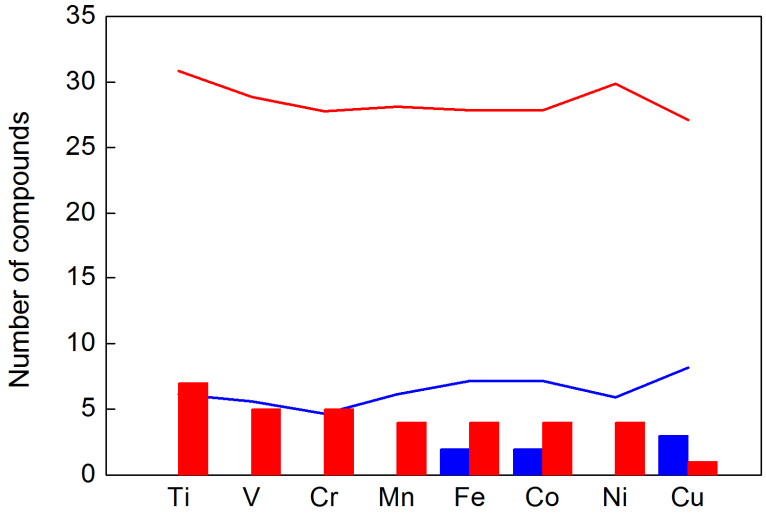

Figure 3.2 A number of trivalent compounds with coordination numbers 4 and 6. The blue bar shows the number of compounds with coordination number 4 in compounds with negative formation energy. The red bar shows the number of compounds with coordination number 6 in compounds with negative formation energy. The blue line shows the number of compounds with coordination number 4 in all calculated compounds. The red line shows the number of compounds with coordination number 6 in all calculated compounds.

Figures 4.1 and 4.2 show bond length distribution at each coordination number. Orange closed circles corresponded to the formation energies < 0eV/cation. Light-blue closed circles corresponded to the formation energies between 0 to 0.1eV/cation. Dark-blue closed circles corresponded to the formation energies > 0.1eV/cation.

Figure 4.1 shows bond length distribution of each coordination number at phase relationships in pseudo-ternary systems of $1/2Li_2O$-MO-$1/2P_2O_5$. The each graph shows titanium (a), vanadium (b), chromium (c), manganese (d), iron (e), cobalt (f), nickel (g), copper (h), zinc (i) and magnesium (j). The bond length tended to increase with increasing coordination number. Dispersion of the bond length distribution in compounds with negative formation energy was smaller than dispersion of the bond length in compounds with positive formation energy.

This study used a value of 1.26 Å for the O^{2-} ion. This value is referred to as Shannon crystal radii. A bond length was represented as the sum of Shannon crystal radius of cation and oxygen. In the coordination number 4, the bond length of Mn^{2+}-O, Fe^{2+}-O, Co^{2+}-O, Ni^{2+}-O, Cu^{2+}-O and Zn^{2+}-O were 2.06Å, 2.03Å, 1.98Å, 1.95Å, 1.97Å and 2Å respectively. In the coordination number 5, the bond length of Mn^{2+}-O, Co^{2+}-O, Ni^{2+}-O, Cu^{2+}-O and Zn^{2+}-O were 2.15Å, 2.07Å, 2.05Å, 2.05Å and 2.08Å respectively. In the coordination number 6, the bond length of Ti^{2+}-O, V^{2+}-O ,Cr^{2+}-O, Mn^{2+}-O, Fe^{2+}-O, Co^{2+}-O, Ni^{2+}-O, Cu^{2+}-O and

Zn^{2+}-O were 2.26Å, 2.19Å, 2.2Å, 2.23Å, 2.18Å, 2.15Å, 2.09Å, 2.14Å and 2.13Å respectively. The M-O bond lengths calculated by first principle calculations did not contradict an experimental data. These bond lengths were included in bond lengths with calculated compounds. Especially bond lengths with negative formation energy were good agreement with Shannon crystal radii.

Figure 4.2 shows bond length distribution of each coordination number at phase relationships in pseudo-ternary systems of $1/2Li_2O$-$1/2M_2O_3$-$1/2P_2O_5$. The each graph shows titanium (a), vanadium (b), chromium (c), manganese (d), iron (e), cobalt (f), nickel (g), and copper (h). Dispersion of the bond length distribution in compounds with negative formation energy was smaller than dispersion of the bond length in compounds with positive formation energy.

In the coordination number 4, the bond length of Fe^{3+}-O was 1.89Å. In the coordination number 5, the bond length of Mn^{3+}-O, Fe^{3+}-O were 1.98Å and 1.98Å respectively. In the coordination number 6, the bond length of Ti^{2+}-O, V^{2+}-O ,Cr^{2+}-O, Mn^{2+}-O, Fe^{2+}-O, Co^{2+}-O, Ni^{2+}-O, and Cu^{2+}-O were 2.07Å, 2.04Å, 2.02Å, 2.05Å, 2.05Å, 2.01Å, 2.00Å and 1.94Å respectively. The M-O bond lengths calculated by first principle calculations did not contradict an experimental data. These bond lengths were included in bond lengths with calculated compounds. Especially bond lengths with negative formation energy were good agreement with Shannon crystal radii.

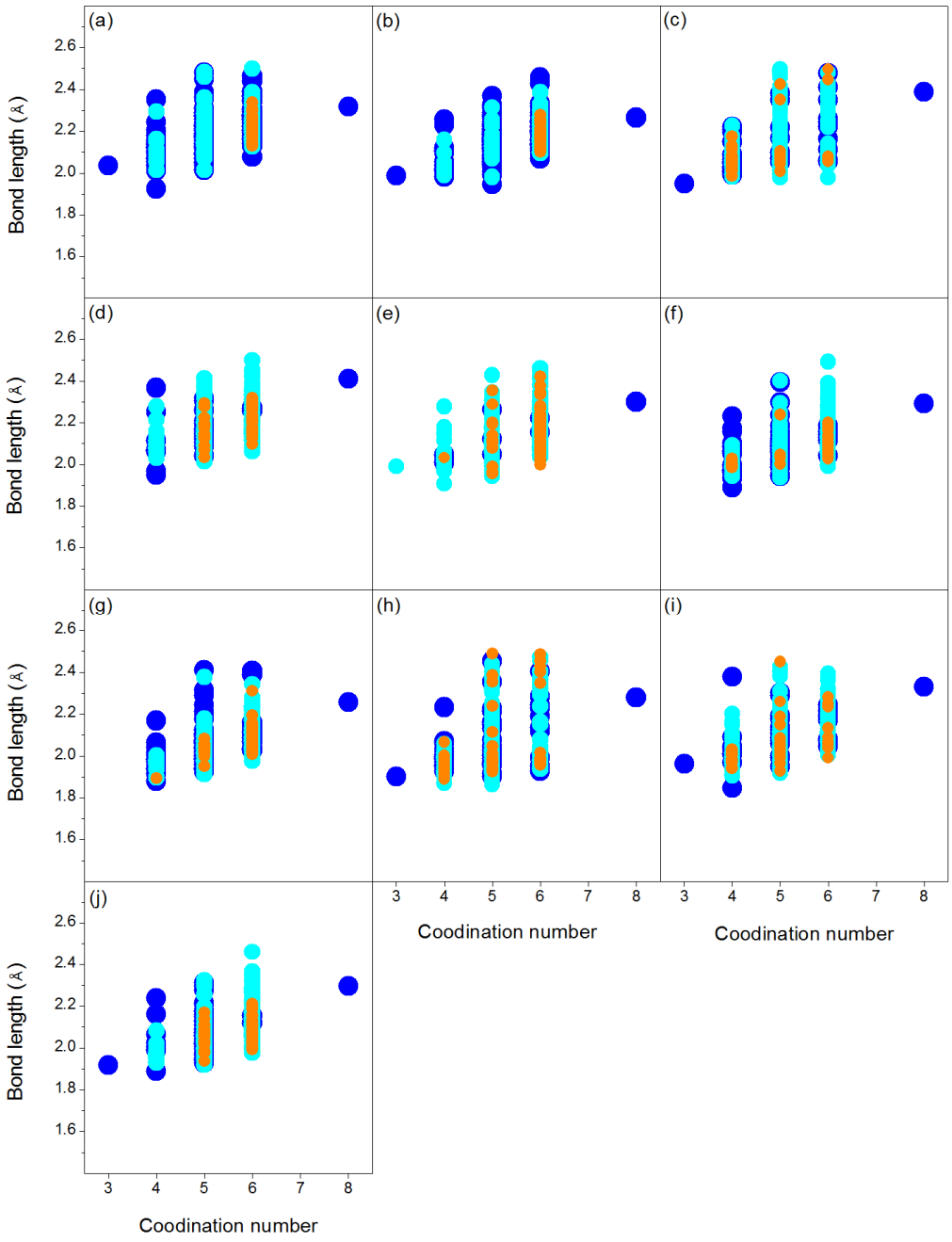

Figure 4.1 M-O bond length vs. coordination number of divalent cations in all divalent compounds, M = (a)Ti^{2+}, (b)V^{2+}, (c)Cr^{2+}, (d)Mn^{2+}, (e)Fe^{2+}, (f)Co^{2+}, (g)Ni^{2+}, (h)Cu^{2+}, (i)Zn^{2+} and (j)Mg^{2+}. Orange closed circles corresponded to the formation energies < 0eV/cation. Light-blue closed circles corresponded to the formation energies between 0 to 0.1eV/cation. Dark-blue closed circles corresponded to the formation energies > 0.1eV/cation.

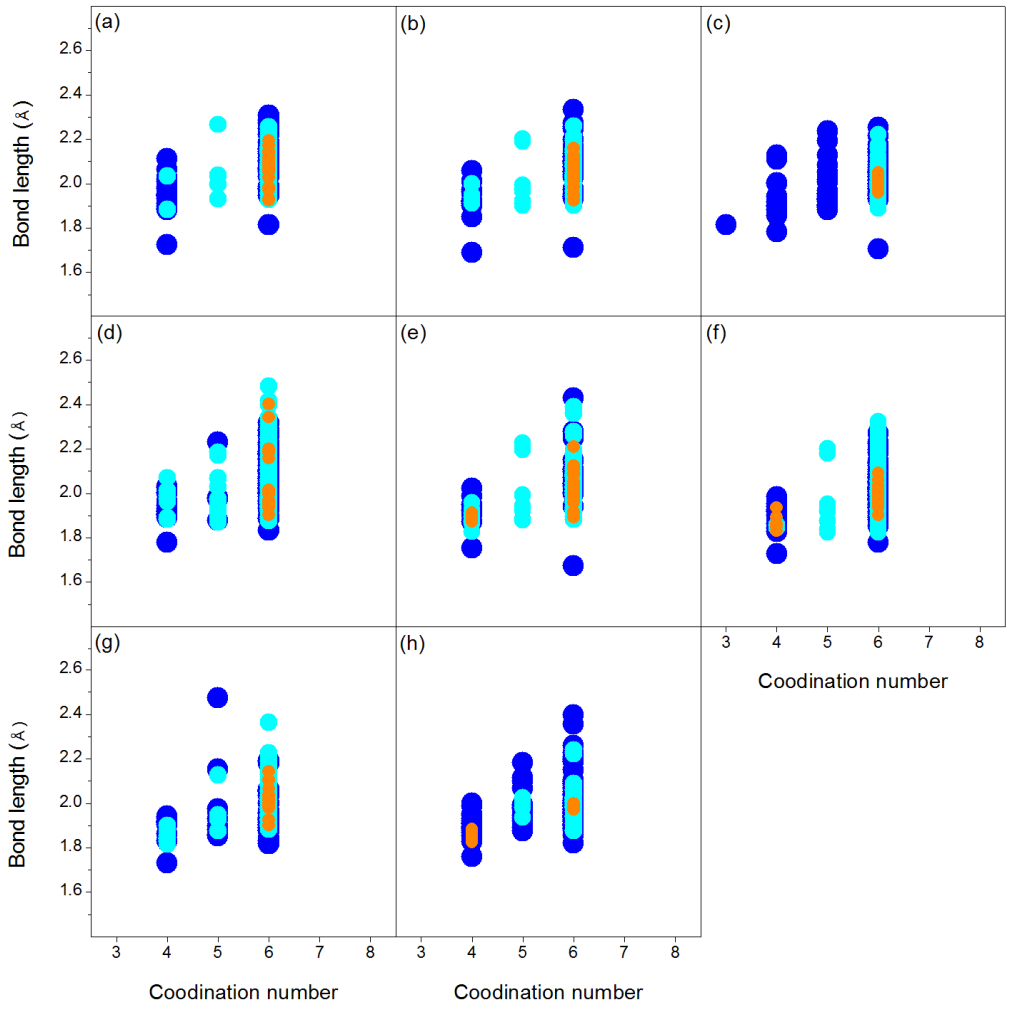

Figure 4.2 M-O bond length vs. coordination number of trivalent cations in all trivalent compounds, M = (a)Ti^{3+}, (b)V^{3+}, (c)Cr^{3+}, (d)Mn^{3+}, (e)Fe^{3+}, (f)Co^{3+}, (g)Ni^{3+} and (h)Cu^{3+}. Orange closed circles corresponded to the formation energies < 0eV/cation. Light-blue closed circles corresponded to the formation energies between 0 to 0.1eV/cation. Dark-blue closed circles corresponded to the formation energies > 0.1eV/cation.

Figure 5.1 and Figure 5.2 show bond length between lithium and oxygen. These bond lengths had wide distribution at each coordination number and bond length distributions did not depend on the formation energy. According to Shannon crystal radii, the ionic radius of lithium with coordination number 4 is 0.73Å and the ionic radius of oxygen is 1.26Å. Hence bond length between lithium and oxygen is 1.99Å. However some of calculated bond lengths were 2.1Å or more. The calculated bond length was not good agreement with Shannon crystal radii. The coordination number of the oxygen bonded to lithium had some variation and bond length between lithium and oxygen did not depend on the coordination number.

Figure 6.1 and Figure 6.2 indicate that a phosphorus had an oxygen coordination number 4 (i.e. PO4 unit). This bond length was constant value at all calculated compounds. Nevertheless, all calculated compounds included the thermodynamically unstable compounds. These bond lengths were from 1.46Å to 1.67Å. In Shannon crystal radii, ionic radius of phosphorous is 0.31Å and ionic radius of oxygen is 1.26Å. Hence bond length between phosphorous and oxygen became 1.57Å. The calculated bond length was good agreement with Shannon crystal radii. This calculation results are 6% or more and 7% or less of the Shannon crystal radii.

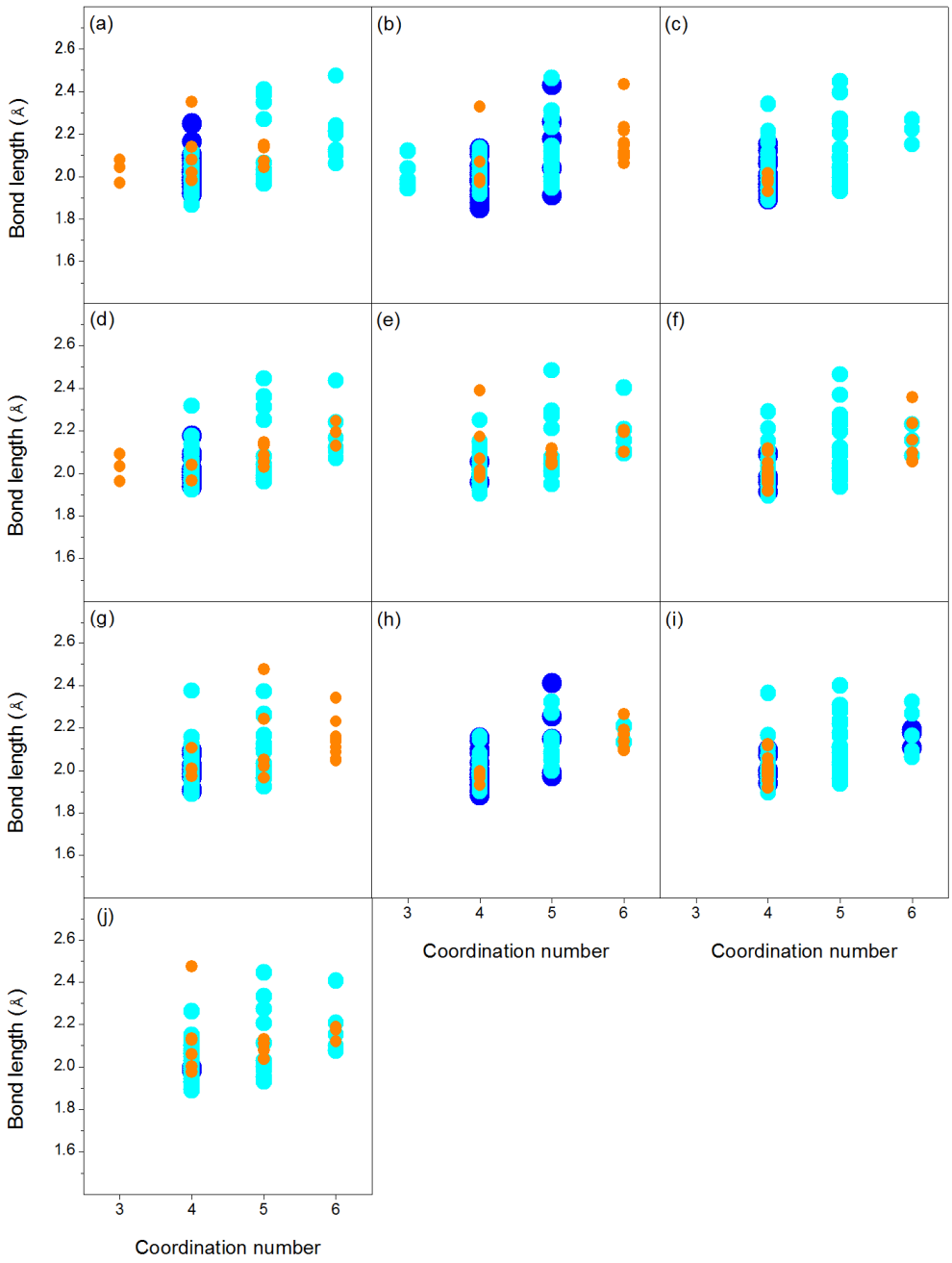

Figure 5.1 Li-O bond length vs. coordination number of divalent cations in all divalent compounds, M = (a)Ti^{2+}, (b)V^{2+}, (c)Cr^{2+}, (d)Mn^{2+}, (e)Fe^{2+}, (f)Co^{2+}, (g)Ni^{2+}, (h)Cu^{2+}, (i)Zn^{2+} and (j)Mg^{2+}. Orange closed circles corresponded to the formation energies < 0eV/cation. Light-blue closed circles corresponded to the formation energies between 0 to 0.1eV/cation. Dark-blue closed circles corresponded to the formation energies > 0.1eV/cation.

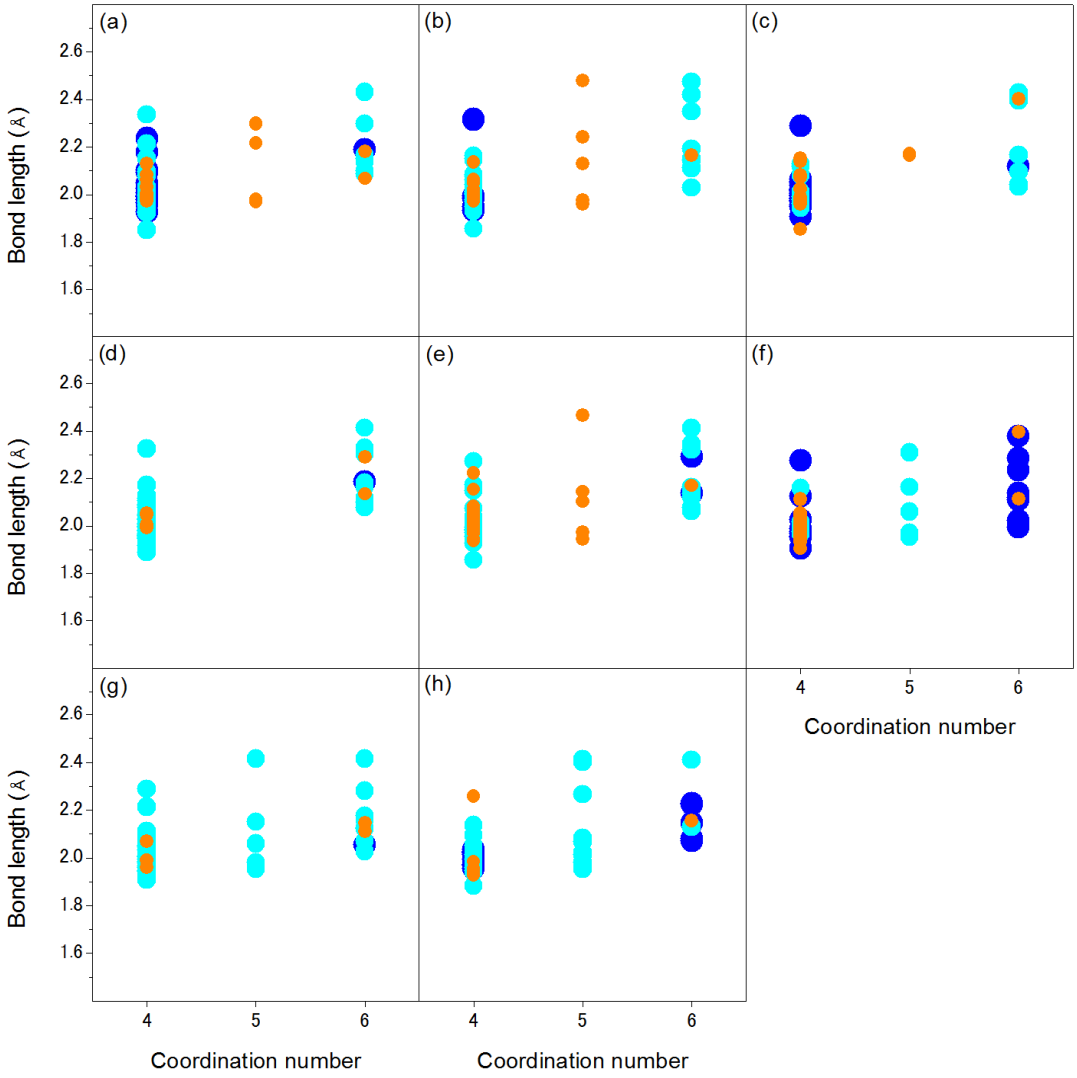

Figure 5.2 Li-O bond length vs. coordination number of trivalent cations in all trivalent compounds, M = (a)Ti^{3+}, (b)V^{3+}, (c)Cr^{3+}, (d)Mn^{3+}, (e)Fe^{3+}, (f)Co^{3+}, (g)Ni^{3+} and (h)Cu^{3+}. Orange closed circles corresponded to the formation energies < 0eV/cation. Light-blue closed circles corresponded to the formation energies between 0 to 0.1eV/cation. Dark-blue closed circles corresponded to the formation energies > 0.1eV/cation.

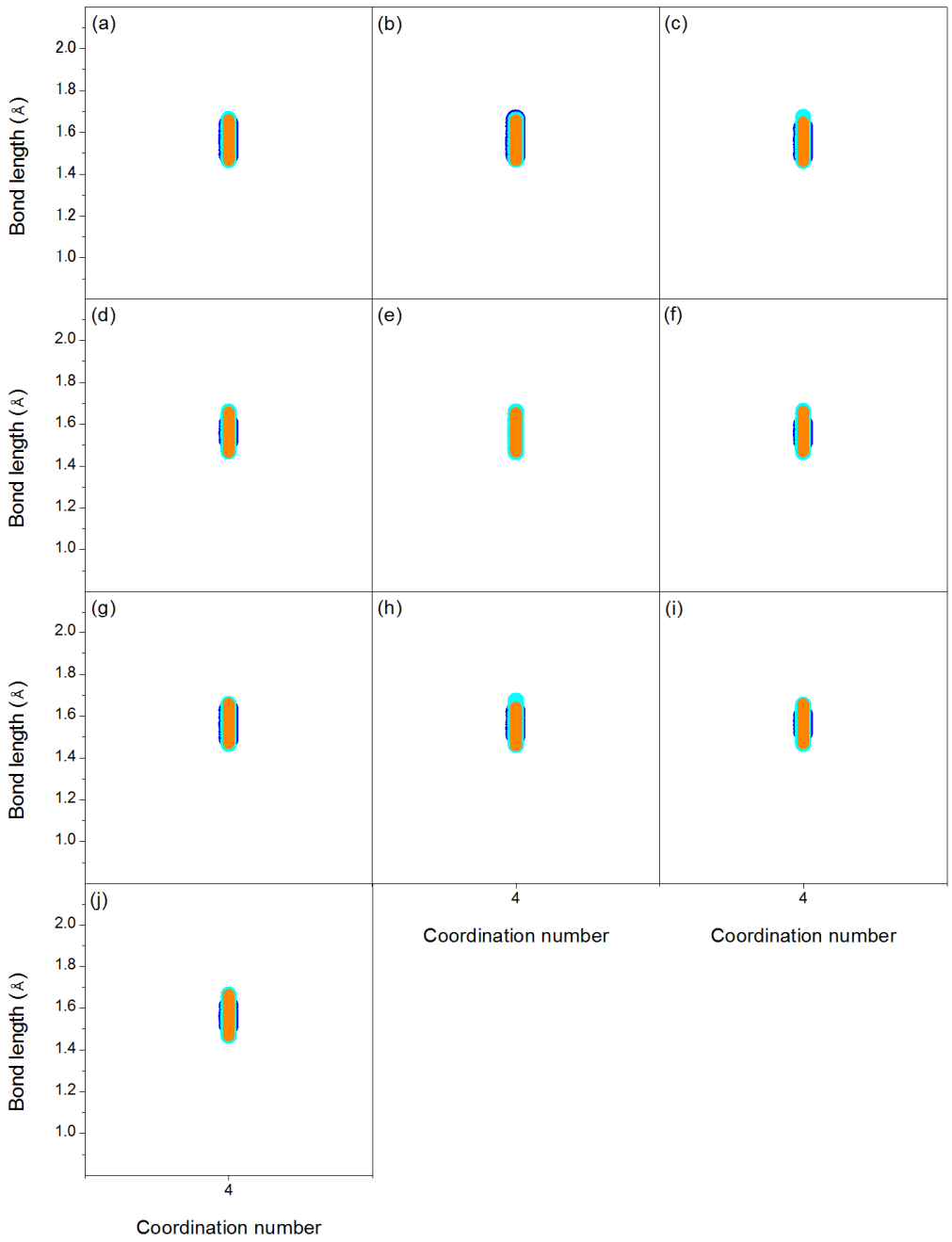

Figure 6.1 P-O bond length vs. coordination number of divalent cations in all divalent compounds, M = (a)Ti^{2+}, (b)V^{2+}, (c)Cr^{2+}, (d)Mn^{2+}, (e)Fe^{2+}, (f)Co^{2+}, (g)Ni^{2+}, (h)Cu^{2+}, (i)Zn^{2+} and (j)Mg^{2+}. Orange closed circles corresponded to the formation energies < 0eV/cation. Light-blue closed circles corresponded to the formation energies between 0 to 0.1eV/cation. Dark-blue closed circles corresponded to the formation energies > 0.1eV/cation.

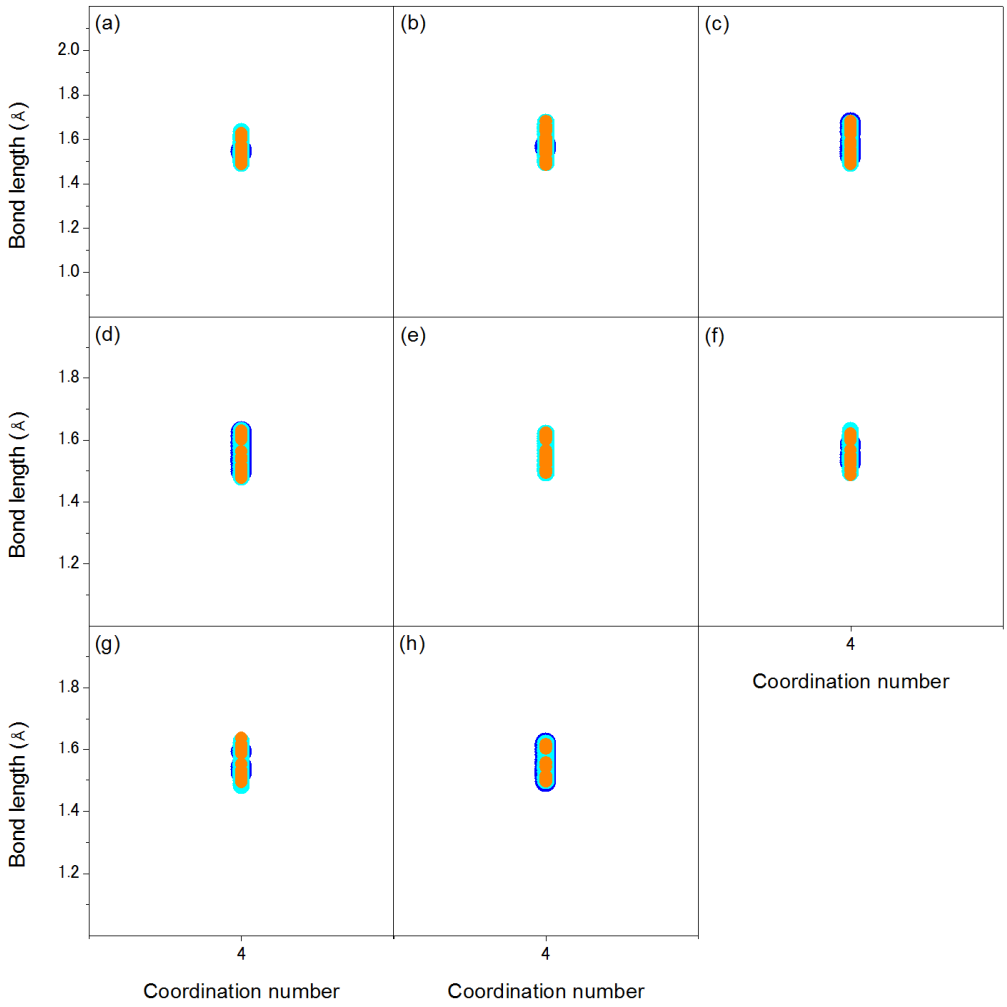

Figure 6.2 P-O bond length vs. coordination number of trivalent cations in all trivalent compounds, M = (a)Ti^{3+}, (b)V^{3+}, (c)Cr^{3+}, (d)Mn^{3+}, (e)Fe^{3+}, (f)Co^{3+}, (g)Ni^{3+} and (h)Cu^{3+}. Orange closed circles corresponded to the formation energies < 0eV/cation. Light-blue closed circles corresponded to the formation energies between 0 to 0.1eV/cation. Dark-blue closed circles corresponded to the formation energies > 0.1eV/cation.

Figure 7.1 shows relationship between Li/Cation ratio and cell volume in all calculated compounds. Figure 7.2 shows relationship between P/Cation ratio and cell volume in all calculated compounds. As can be seen from figures 7.1 and 7.2, cell volume was related to Li/cation ratio and P/cation ratio. The cell volume tended to decrease with decreasing Li/Cation ratio. On the other hand, the cell volume tended to increase with increasing P/Cation ratio.

At Li=0, P=0 and P=0.5, dispersion of cell volume is wide. This results were linked to coordination number and bond length of transition metal. Figure 8 shows the relationship among coordination number, bond length and volume at transition metal oxides. These plots contained not only thermodynamically stable structures but also thermodynamically unstable structures. One structure had some atoms and a number of atoms were different at each structure. Bond lengths were used the average value and volumes were used volume per cation. Figure 8 (a) shows the relationship among bond lengths, coordination numbers and volumes in the simple metal oxides of divalent compounds. Figure 8 (b) shows the relationship among bond lengths, coordination numbers and volumes in the simple metal oxides of trivalent compounds. The structure of divalent elements had the coordination number 4, 6 and 8. The structure of trivalent elements had the coordination number only 6. The coordination number increased when the bond length increased.

At the coordination number 4, maximum bond length was 2.10Å and minimum bond length was 1.94Å. At the coordination number 6, maximum bond length was 2.27Å and minimum bond length was 2.11Å. At the coordination number 8, maximum bond length was 2.41Å and minimum bond length was 2.26Å. This result indicates that

maximum bond length of coordination number 4 was nearly equal to minimum bond length of coordination number 6 and maximum bond length of coordination number 6 was nearly equal to minimum bond length of coordination number 8. It seems that each coordination number had a threshold bond length. The threshold value changed from coordination number 4 to coordination number 6 was 2.11Å and the threshold value changed from coordination number 6 to coordination number 8 was 2.27Å.

At same coordination number, the volume was proportional to bond length. Compared with Figure 8 (a) and Figure 8 (b), the structures of trivalent element had lower distance and higher volume. This result caused by a number of oxygen atoms. These volumes were used per cation. Hence a number of oxygen atoms per cation were different so a number of oxygen at trivalent oxides was 1.5 times than a number of oxygen at divalent oxides. If volume standardize at a number of atoms, volume was proportional to bond length.

At same bond length, the volume was high if the coordination number was low. The volume of each structure was linked to a kind of transition metals. The elements of higher volume were chromium and manganese. The structure of manganese had highest volume at all coordination numbers. On the other hand, the elements of lower volume were nickel and copper. The structure of Nickel had lowest volume at all coordination number.

Second we focused on the lithium transition metal oxides. Figure 11 shows the relationship among coordination numbers, bond lengths and volumes at lithium transition metal oxides. Figure 9 (a) shows the relationship among bond lengths, coordination numbers and volumes in the lithium transition metal oxides of divalent

compounds and Figure 9 (b) shows the relationship among bond lengths, coordination numbers and volumes in the lithium transition metal oxides of trivalent compounds.. The closed circle was coordination number 4 and the closed square is coordination number 6. At lithium transition metal oxides, coordination number 8 did not exist. At the coordination number 4, higher lithium ratio was orange closed circle and pink closed circle. The middle lithium ratio was light-blue closed circle and light-green closed circle, and the lower lithium ratio was blue closed circle and green closed circle.

The lithium per cation ratio of orange closed circle was 0.909, that of light-blue closed circle was 0.857 and that of blue closed circle was 0.667. The highest volume structure was the lowest lithium per cation ratio, but the lowest volume structure was not highest lithium per cation ratio. The lithium per cation ratio of pink closed circle was 0.833, that of light-green closed circle was 0.75 and that of green closed circle was 0.5. The highest volume structure was the lowest lithium ratio, but the lowest volume structure was highest lithium ratio. Lithium ratio was related to volume. It seems that lithium is closed the unoccupied site, so volume per cation was decrease at high lithium ratio. The coordination number increased when the bond length increased. This trend was similar to the simple oxide.

Therefore it is apparent that coordination number and bond length of transition metal was linked to cell volume but was not dominant factor.

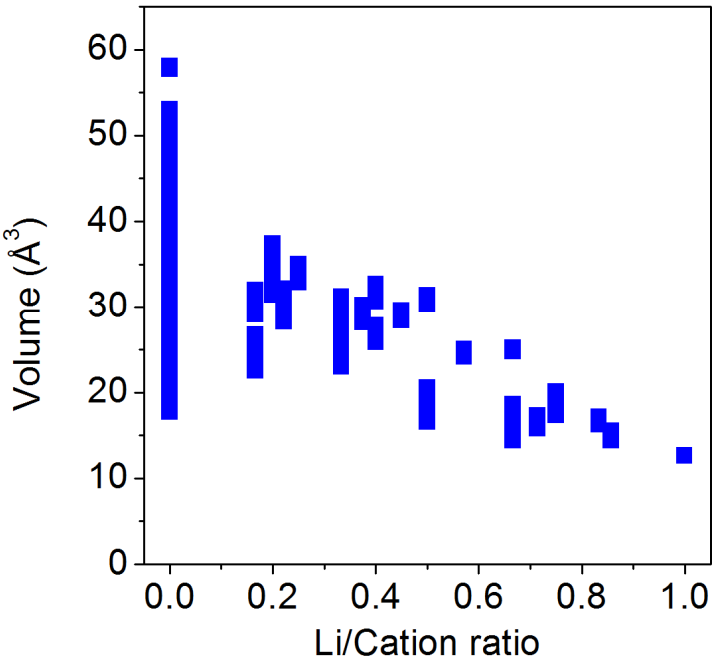

Figure 7.1 Relationship between Li/Cation ratio and cell volume in all calculated compounds.

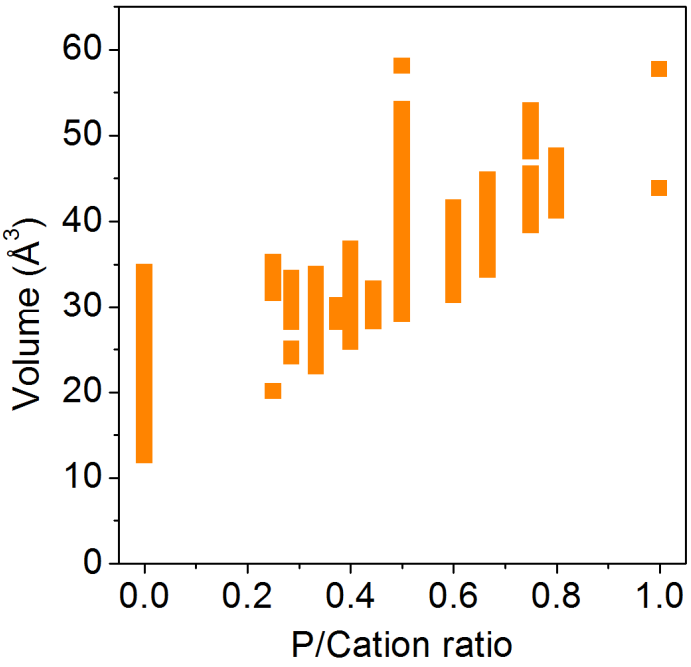

Figure 7.2 Relationship between P/Cation ratio and cell volume in all calculated compounds.

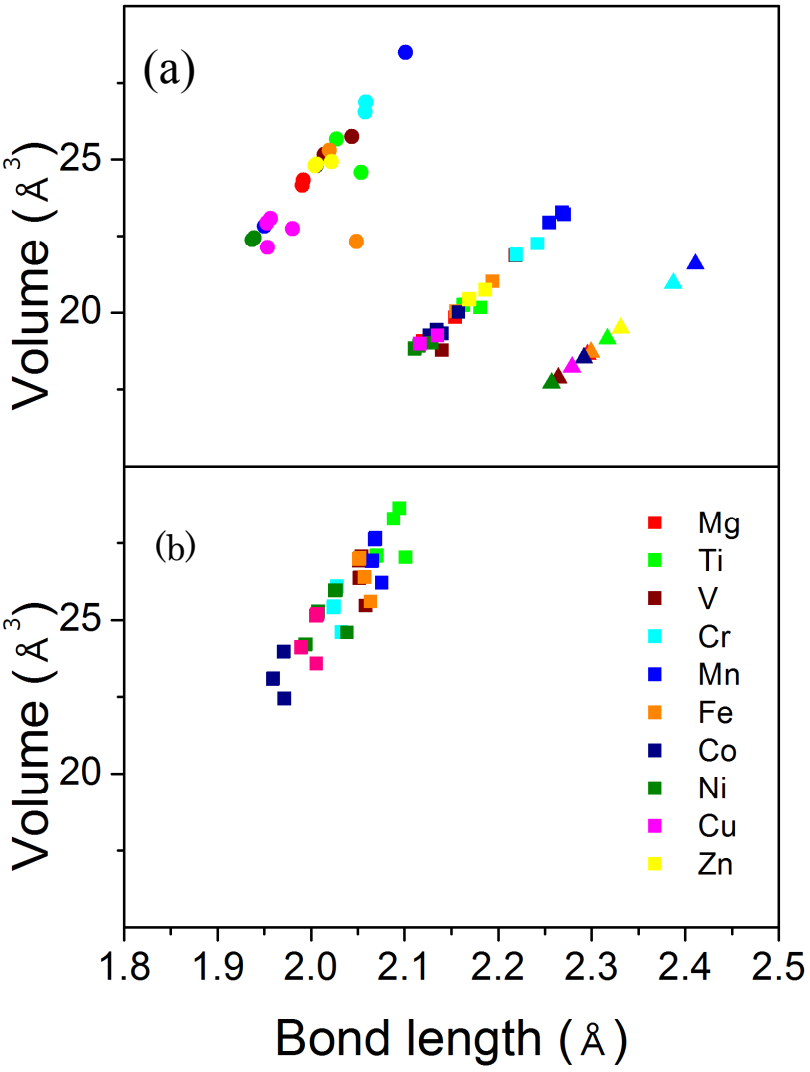

Figure 8 Relationship among bond lengths, coordination numbers and volumes in the simple metal oxides of (a) divalent compounds and (b) trivalent metal compounds.. Closed circles, closed squares and closed triangles denote coordination number 4, 6 and 8 respectively.

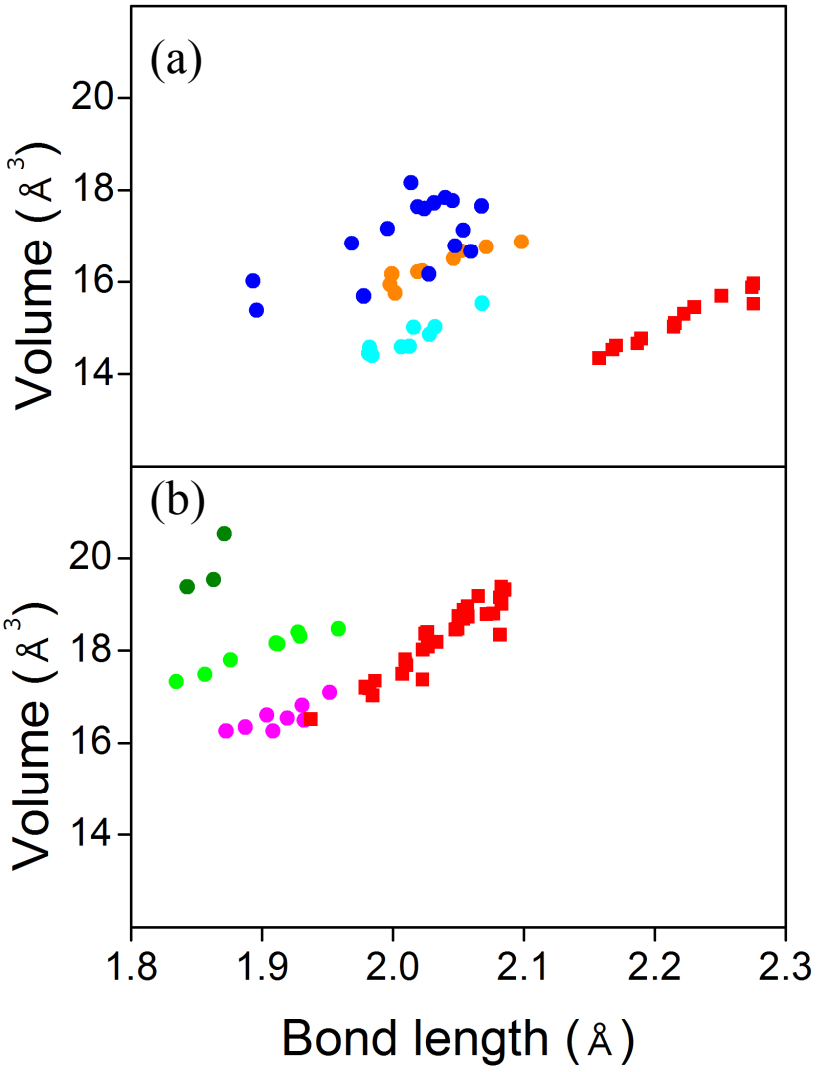

Figure 9 Relationship among bond lengths, coordination numbers and volumes in the lithium transition metal oxides of (a) divalent compounds and (b) trivalent compounds. The closed square is coordination number 6 and the closed circle is coordination number 4. Orange closed circles were Li/cation ratio = 0.909, light-blue closed circles were Li/cation ratio =0.857 and blue closed circles were Li/cation ratio 0.667. Pink closed circles were Li/cation ratio 0.833, light-green closed circles were Li/cation ratio = 0.75 and green closed circles were Li/cation ratio = 0.5.

Figure 10 shows relationship between O/cation and cell volume. This result indicates that cell volume was proportional to O/Cation. The cell volume tended to decrease with decreasing O/Cation ratio. On the other hand, the cell volume tended to increase with increasing O/Cation ratio. O/Cation ratio was link to Li/Cation ratio and P/Cation ration. Li/Cation ratio tended to decrease with decreasing O/Cation ratio. On the other hand, P/Cation ration tended to increase with increasing O/Cation ratio.

Therefore O/Cation ratio is the useful parameter in phosphate materials. This parameter predicts the cell volume.

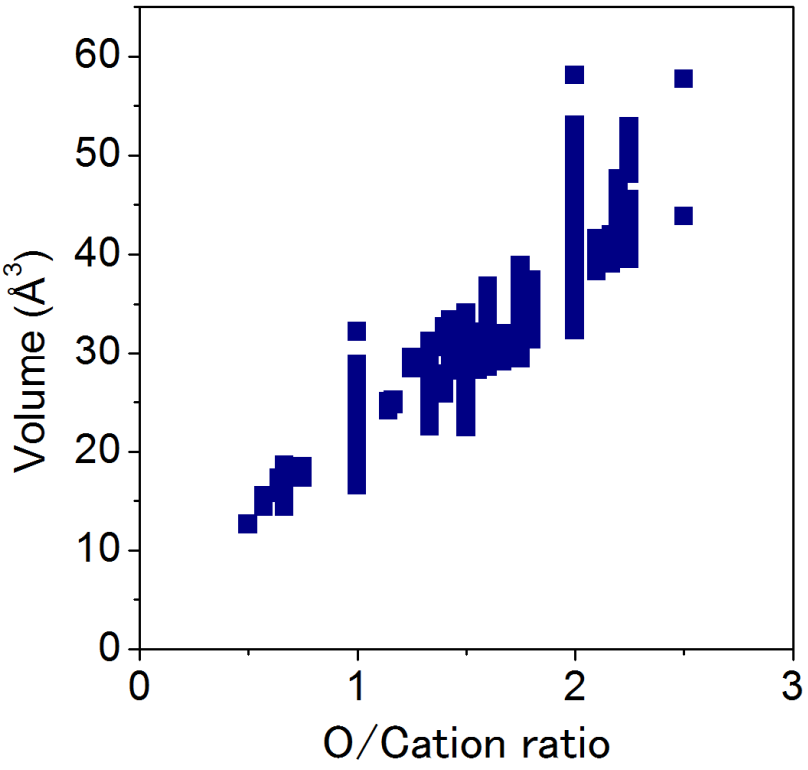

Figure 10 Relationship between Li/Cation ratio and cell volume in all calculated compounds.

3-4 Summary

1. This work performed the comparative study of crystal structures of lithium metal phosphates. This comparative study used not only thermodynamically stable structures but also thermodynamically unstable structures.
2. Dispersion of the M-O bond length distribution in compounds with negative formation energy was smaller than dispersion of the M-O bond length in compounds with positive formation energy.
3. The M-O bond lengths calculated by first principle calculations did not contradict an experimental data.
4. These Li-O bond lengths had wide distribution at each coordination number and Li-O bond length distributions did not depend on the formation energy.
5. This P-O bond length was constant value at all calculated compounds. Nevertheless, all calculated compounds included the thermodynamically unstable compounds.
6. At the phosphates, cell volume was proportional to O/cation ratio.

References

[1] A. S. Andersson, J. O. Thomas, B. Kalska and L. Häggströmb, Electrochem. Solid-State Lett., 3(2), 66-68 (2000)

[2] M. Takahashi, H. Ohtsuka, K. Akuto and Y. Sakurai. Electrochem. Soc., 152(5), A899-A904 (2005)

[3] A.K.Padhi, K.S.Nanjundaswamy and J. B. Goodenough, Electrochem. Soc., 144(4), 1188-1194 (1997)

[4] N. Ravet, Y. Chouinard, J.F. Magnan, S. Besner, M. Gauthier, M. Armand, J. Power Sources, 97–98, 503-507 (2001)

[5] H. Aono, E. Sugimoto, Y. Sadaoka, N. Imanaka and G. Adachi, J. Electrochem. Soc., 137(4), 1023-1027 (1990)

[6] G. Hautier, A. Jain, S. P. Ong, B. Kang, C. Moore, R. Doe, and G. Ceder, Chem. Mater., 23, 3495 – 3508 (2011)

[7] H. Zhou,S. Upreti,N. A. Chernova, G. Hautier, G. Ceder and M. S. Whittingham, Chem. Mater., 23, 293–300 (2011)

[8] Y. Mo, S. P. Ong and G. Ceder, Chem. Mater., 24, 15−17 (2012)

[9] D. Morgan, G. Ceder, M. Y. Saidi, J. Barker, J. Swoyer, H. Huang, G. Adamson. Chem. Mater., 14(11), 4684-4693 (2002)

[10] D. Morgan, G. Ceder, M. Y. Saidi, J. Barker, J. Swoyer, H. Huang and G. Adamson, J. Power Sources, 119, 755-759 (2003)

[11] D. Morgan, A. Van der Ven and G. Ceder, Electrochem. Solid State Lett., 7(2), A30-A32 (2004)

[12] F. Zhou, C.A. Marianetti, M. Cococcioni, D. Morgan and G. Ceder, Phys. Rev. B, 69, 201101 (2004)

[13] F. Zhou, K. Kang, T. Maxisch, G. Ceder and D. Morgan, Solid State Comm., 132, 181-186 (2004)

[14] T. Maxisch, F. Zhou and G. Ceder, Phys. Rev. B, 73, 104301 (2006)

[15] T. Maxisch and G. Ceder, Phys. Rev. B, 73, 174112 (2006)

[16] F. Zhou, T. Maxisch and G. Ceder, Phys. Rev. Lett., 97, 155704 (2006)

[17] L. Wang, F. Zhou, Y.S. Meng and G. Ceder, Phys. Rev. B, 76, 16435 (2007)

[18] S. P. Ong, L. Wang, B. Kang and G. Ceder. Chem. Mater., 20(5), 1798-1807 (2008)

[19] L. Wang, F. Zhou and G. Ceder. Electrochem. Solid-State Lett., 11(6), A94-A96 (2008)

[20] R. Malik, F. Zhou and G. Ceder, Phys. Rev. B, 79, 214201 (2009)

[21] S. P. Ong, A. Jain, G. Hautier, B. Kang and G. Ceder. Electrochem. Comm., 12(3), 427-430 (2010)

[22] S. P. Ong, V. L Chevrier and G. Ceder. Phys. Rev. B, 83(075112), 1-7 (2011)

[23] H. Zhou, S. Upreti, N.A. Chernova, G. Hautierand, G. Ceder and M. S. Whittingham, Chem. Mater., 23(2), 293-300 (2011).

[24] A. Jain, G. Hautier, C. Moore, B. Kang, J. Lee, H. Chen, N. Twu and G. Ceder, J. Electrochem. Soc., 159(5), A622-A633 (2012).

[25] K. Rajan, Mater. Today, 8(10), 38-45 (2005)

[26] S. Curtarolo et al. Nature Mater., 12, 191–201 (2013)

[27] G. Ceder, MRS Bulletin, 35, (2010)

[28] G. Hautier, A. Jain, H. Chen, C. Moore, S. P. Ong and G. Ceder, J. Mater. Chem., 21, 17147-17153 (2011)

[29] R. Jalem, T. Aoyama, M. Nakayama and M. Nogami, Chem. Mater., 24, 1357−1364 (2012)

[30] J. P. Perdew, K. Burke and M. Ernzerhof, Phys. Rev. Lett., 77(18) 3865-3868 (1996)

[31] G. Kresse and J. Furthmuller, Phys. Rev. B, 54 (16) 11169-11186 (1996)

[32] P. E. Blochl, Phys. Rev. B, 50 (24) 17953-17979 (1994)

[33] V. I Anisimov, F Aryasetiawan and A I Lichtenstein, J. Phys.: Condens. Matter, 9, 767–808 (1997)

[34] V. I. Anisimov, J. Zaanen and O. K. Andersen, Phys. Rev. B, 44(3) 943-954 (1991)

[35] F. Zhou, M. Cococcioni, C. A. Marianetti, D. Morgan, and G. Ceder, Phys. Rev. B, 70, 235121 (2004)

[36]W. Setyawan, R. M. Gaume, S. Lam, R. S. Feigelson and S. Curtarolo, ACS Comb. Sci., 13, 382–390 (2011)

[37] H. J. Monkhorst and J. D. Pack, Phys. Rev. B, 13, 5188 (1976)

[38] R. D. Shannon, Acta Cryst., A32, 751-767 (1976)

Chapter 4
Factors determining redox potential of lithium metal phosphates

4-1 Introduction

Lithium-ion batteries play important roles in modern technology. The advantages of lithium-ion battery as compared to other batteries are high-energy density, high-power density, low self-discharge and high efficiency between charge and discharge. Thanks to such properties, lithium-ion batteries have been used for not only portable devices but also large-scale electricity storages. The disadvantage of lithium-ion battery is safety. Lithium-ion batteries may explode when exposed to high temperatures [1-4]. Oxygen release by thermal decomposition of cathode oxides is the major source of the explosion [5-8]. Hence the search of better cathodes materials with improved safety is an important issue for future development of lithium ion batteries. At the present, only a few oxides with three structures are practically used as the cathode material. They are layered structure, spinel structure and olivine structure. The cathode material with layered structure such as $LiCoO_2$ [9] is most popular. The spinel structure includes $LiMn_2O_4$ [10] [11]. $LiFePO_4$ has the olivine structure [12], which is also widely used commercially.

Lithium iron phosphate for cathode material have received much attention in recent year due to their high safety and high cycling stability. Lithium-ion batteries can explode when exposed to high temperature. Oxygen release by thermal decomposition of cathode is a potential source of that explosion. Phosphates have strong P-O covalent bonds, so lithium metal phosphates are expected to avoid the oxygen release.

Some of the lithium metal phosphates were also investigated by first principle calculations. Ceder and his coworkers reported many cathode materials for lithium-ion batteries[13-28]. Furthermore some computed phase diagrams are available on the open website of “Material Project”. These results indicate that redox potential of cathodes materials are strongly related to species of transition element and their valence. High-throughput screening has been attempted based upon such theoretical database to explore new cathode materials for lithium-ion batteries [29] [30]. However, an alternative cathode material for currently available ones with improved properties has not been discovered.

The purpose of this study is to investigate the relationship between redox potential and fundamental structural data in lithium transition metal phosphates. This comparative study aims to lead us to discover new cathode materials based upon the information by first principle calculations.

4-2 Method

In this work, the relationship between electronic property and fundamental structural data was investigated by first principle calculations. Pseudo-ternary systems of $1/2Li_2O$-MO-$1/2P_2O_5$ and $1/2Li_2O$-$1/2M_2O_3$-$1/2P_2O_5$ were focused on this study. The

divalent element is selected from Mg, Ti, V, Cr, Mn, Fe, Co, Ni, Cu and Zn. The trivalent element is selected from Ti, V, Cr, Mn, Fe, Co, Ni and Cu. These metals excluding Mg were chosen from period 4 elements. Crystal structures in diagrams were extracted from the inorganic crystal structure database (ICSD). First a phase relationships were constructed by first principle calculations. All compounds were classified into three groups, namely “negative formation energy”, “slightly positive formation energy” and “highly positive formation energy”. Second the fundamental structural data were analyzed at all calculated structures. Finally a redox potential was calculated.

All internal energy were calculated by density functional theory (DFT) using a generalized gradient approximation (GGA) functional parameterized by Perdew, Burke and Ernzerhof (PBE) [31]. All calculations were performed by Vienna ab initio simulation package (VASP) [32] with the projector augmented-wave (PAW) [33] potentials. The plane wave cutoff energy was set at 500eV. Almost all calculations were used with spin polarization and Hubbard *U* parameters for some transition metals. The calculations contained magnesium and zinc were not used with Hubbard *U* parameters. All magnetic moments of transition metals were set initial state to high spin. We used two *U* parameters. One *U* parameter for Ti, V and Cr was 2eV and the other *U* parameter for Mn, Fe, Co, Ni and Cu was 4eV [34-37]. The *k* mesh was sampled according to a Monkhorst-Pack scheme [38] with a spacing of 0.5 /Å.

The voltage was calculated by the chemical potential difference between cathode and anode. The voltage *E* was calculated from the following formula (1) [39] [40].

$$E = -\frac{\mu_{\mathrm{Li}}^{\mathrm{cathode}} - \mu_{\mathrm{Li}}^{\mathrm{anode}}}{zF} \qquad (1)$$

F is the Faraday constant and *z* is the charge transported. In this study the chemical potential of lithium metal was used as the anode.

The theoretical capacity of these cathode materials is calculated the following equation (2).

$$Q = \frac{nF}{M \times 3600} \qquad (2)$$

Q is theoretical capacity typically given in the unit of Ah/g. *F* is the Faraday constant, *n* is the charge transported and *M* is molecular weight.

Table 2 Calculated structures for lithium extraction

Composition	Structure type	Space group	Prototype	Initial valence	Final valence
Li_2MO_2	La_2O_3	*P*-3*m*1	Li_2MnO_2	2	4
	Li_2CuO_2	*Immm*	Li_2CuO_2	2	4
		*C*2/*m*	Li_2CuO_2	2	4
$LiMO_2$	$LiFeO_2$-alpha	$I4_1/amd$	$LiFeO_2$	3	4
	$LiTiO_2$	*Fd*-3*m*	$LiTiO_2$	3	4
	$NaCrS_2$	*R*-3*m*	$LiFeO_2$	3	4
	$NaNiO_2$(mS8)	*C*2/*m*	$LiCuO_2$	3	4
		*Pmm*2	$LiMnO_2$	3	4
$LiMP_3O_9$	$CuLiP_3O_9$	$P2_12_12_1$	$LiFeP_3O_9$	2	3
		P-1	$Cu_2Li_2P_6O_{18}$	2	3
$LiMPO_4$	Mg_2SiO_4	*Pnma*	$LiFe(PO_4)$	2	3
	Na_2CrO_4	*Cmcm*	$LiFe(PO_4)$	2	3
	$LiZnPO_4$	$Pna2_1$	$LiZn(PO_4)$	2	3
		*R*3	$LiZn(PO_4)$	2	3
	$LiGaSiO_4$	*Pnma*	$LiZn(PO_4)$	2	3
$Li_2MP_2O_7$		$P2_1/c$	$Li_2Mn(P_2O_7)$	2	4
	$Na_2PdP_2O_7$	*C*2/*c*	$Li_2Cu(P_2O_7)$	2	4
$LiMP_2O_7$	$LiInP_2O_7$	$P2_1$	$LiFe(P_2O_7)$	3	4

4-3 Results and Discussion

Redox potentials were obtained by first principle calculations. Figure 11 shows relationship between gravimetric capacity and redox potential. Figure 12 shows relationship between volumetric capacity and redox potential. Red closed squares are $LiMO_2$.Pink closed squares are Li_2MO_2. Light green squares are $Li_2MP_2O_7$. Light blue squares are $LiMPO_4$. Green squares are $LiMP_2O_7$. Blue squares are $LiMP_3O_9$. The line shows gravimetric energy density of $LiFePO_4$. These results indicate that $LiMPO_4$ and $Li_2MP_2O_7$ capable of exceeding the energy density of $LiFePO_4$. However these compounds are difficult to exceed the energy density of $LiFePO_4$. Therefore this study attempts to survey the new compositions.

Figure 13 shows the relationship between volume and voltage. This volume was normalized at a number of cation. The closed square is phosphate whose valence changed from +2 or +3 to +4 during charging, the closed triangle is phosphate whose valence changed from +2 to +3 during charging, and the closed circle is oxide whose valence changed from +3 to +4 during charging.

The structures of lithium metal phosphate had a higher volume than those of lithium metal oxides. At a same volume, the redox potential depended on the transition metal element. The structures with titanium and vanadium had lower redox potential. On the other hand, the structures with manganese, cobalt, nickel and copper had higher redox potential. It compared the closed square to the closed triangle at Figure 13. At each transition metal, closed square is higher redox potential than closed triangle. These results were similar to those of earlier experimental and simulation studies.

Figure 13 indicate the redox potential was proportional to volume at each transition

metal. This result shows that the redox potential depends on not only a kind of transition metals but also cell volume. Hence the lithium metal phosphates had higher cell volume and higher redox potential than the lithium metal oxides. Recently some new cathode materials were used nickel as a redox element. Hence redox potential was too high and electrolytes were decomposed. Therefore it is useful to control the redox potential by volume.

Figure 14 (a) shows that the relationship between O/Cation ratio and gravimetric capacity. This figure indicates that the lithium metal phosphate had lower capacity than lithium metal oxide. At the lithium oxides, the higher capacity compound was Li_2MO_2. This compound can transfer the two lithium ions at one molecular. When this compound extracted the lithium, the valence of this compound changed from 2+ to 4+. Figure 14 (b) shows that the relationship between O/Cation ratio and volumetric capacity. When O/Cation ratio is high, P/Cation ratio is high. The chapter 3 shows that the cell volume was related to P/Cation ratio. Therefore volumetric capacity tended to decrease with increasing O/Cation ratio.

Figure 15 shows that the relationship between O/Cation ratio and redox potential. The redox potential tended to increase with increasing the atomic number. At each transition metal, the redox potential tended to increase with increasing O/cation ratio. This result indicates that O/cation is linked to not only volume but also redox potential.

The energy density of cathode material was obtained by redox potential and capacity. Figure 16 shows relationship between O/Cation ratio and gravimetric energy density in all calculated compounds, M = (a)Ti, (b)V, (c)Cr, (d)Mn, (e)Fe, (f)Co, (g)Ni and (h)Cu.

Figure 17 shows relationship between O/Cation ratio and volmetric energy density in all calculated compounds, M = (a)Ti, (b)V, (c)Cr, (d)Mn, (e)Fe, (f)Co, (g)Ni and (h)Cu. These results show that O/cation is linked to energy density. The gravimetric and volumetric energy density tended to decrease with increasing O/Cation ratio.

These results indicate that redox potential and energy density can predict when O/Cation and transition metal are chosen. Our results are encouraging and should be validated in another case.

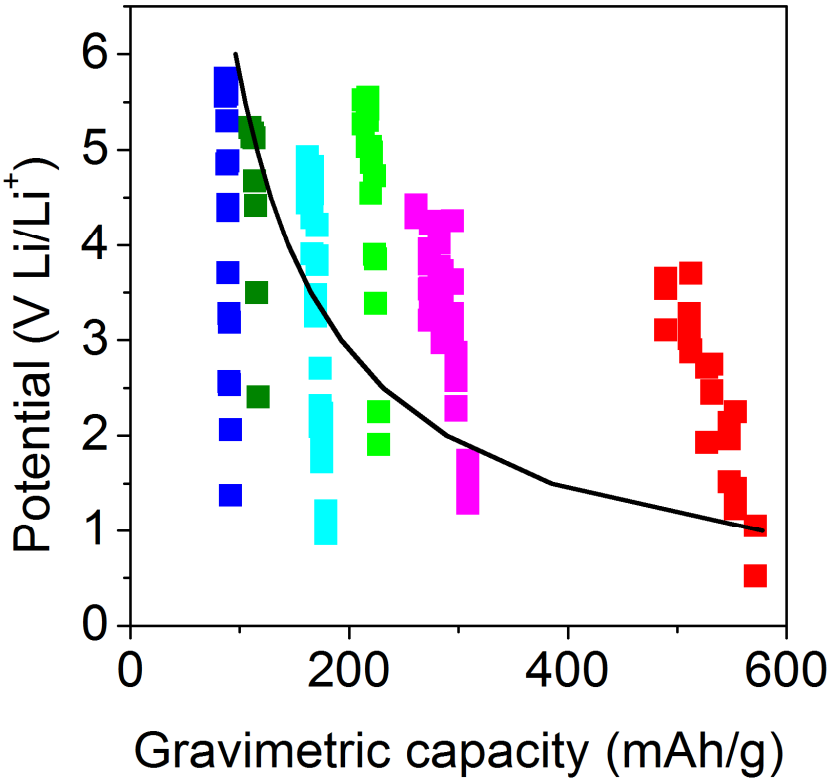

Figure 11 Relationship between gravimetric capacity and redox potential. Red closed squares are $LiMO_2$.Pink closed squares are Li_2MO_2. Light green squares are $Li_2MP_2O_7$. Light blue squares are $LiMPO_4$. Green squares are $LiMP_2O_7$. Blue squares are $LiMP_3O_9$. The line shows gravimetric energy density of $LiFePO_4$.

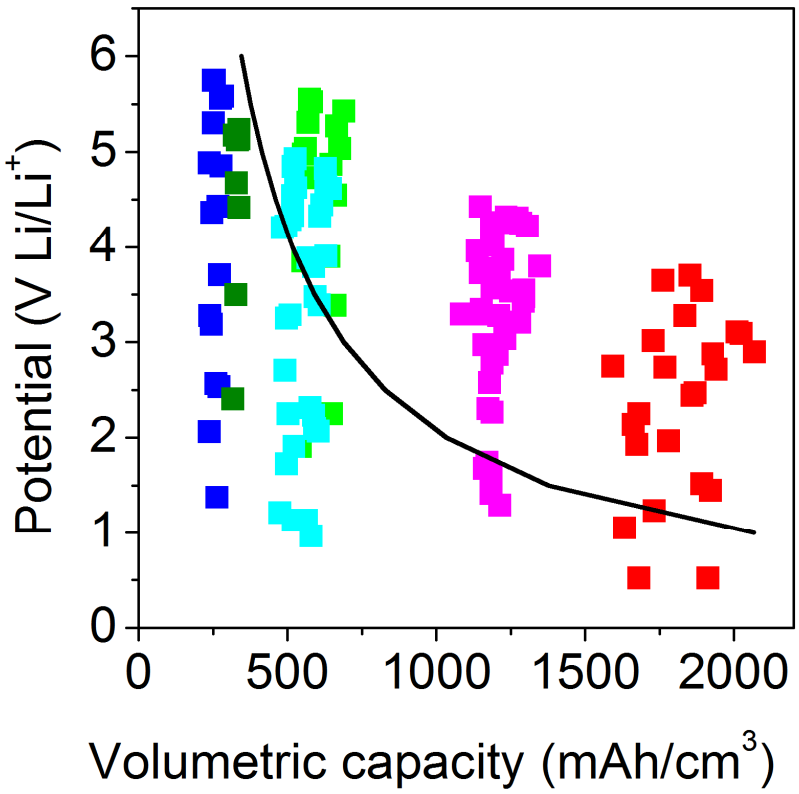

Figure 12 Relationship between volumetric capacity and redox potential. Red closed squares are $LiMO_2$.Pink closed squares are Li_2MO_2. Light green squares are $Li_2MP_2O_7$. Light blue squares are $LiMPO_4$. Green squares are $LiMP_2O_7$. Blue squares are $LiMP_3O_9$. The line shows volmetric energy density of $LiFePO_4$.

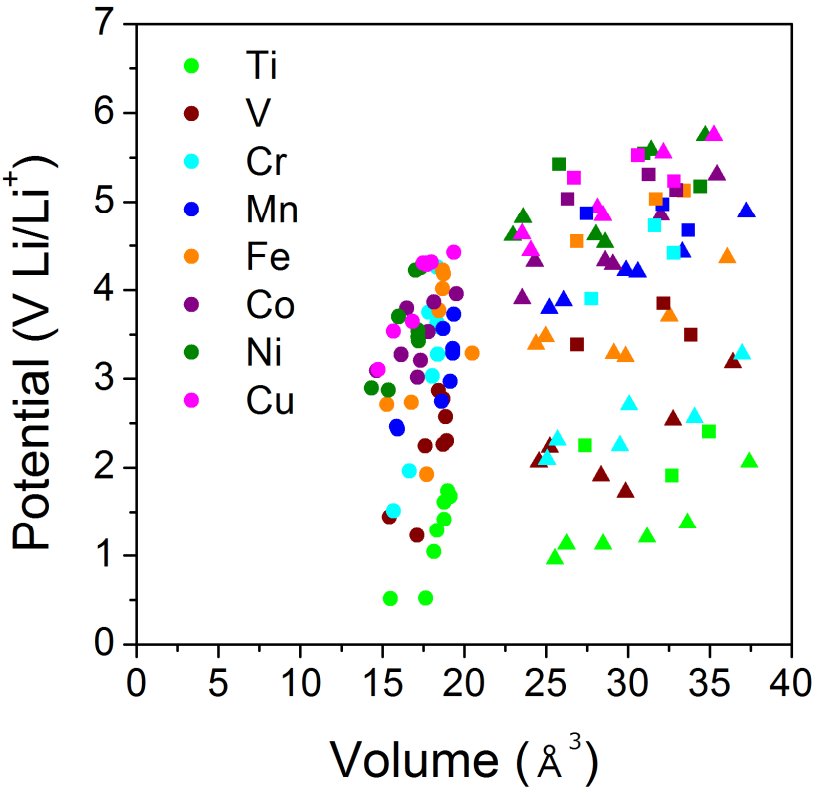

Figure 13 Relationship between volume and voltage on the lithium transition metal phosphates. The closed square is phosphate whose valence changed from +2 to +4 during charging, the closed triangle is phosphate whose valence changed from +2 to +3 during charging, and the closed circle is oxide.

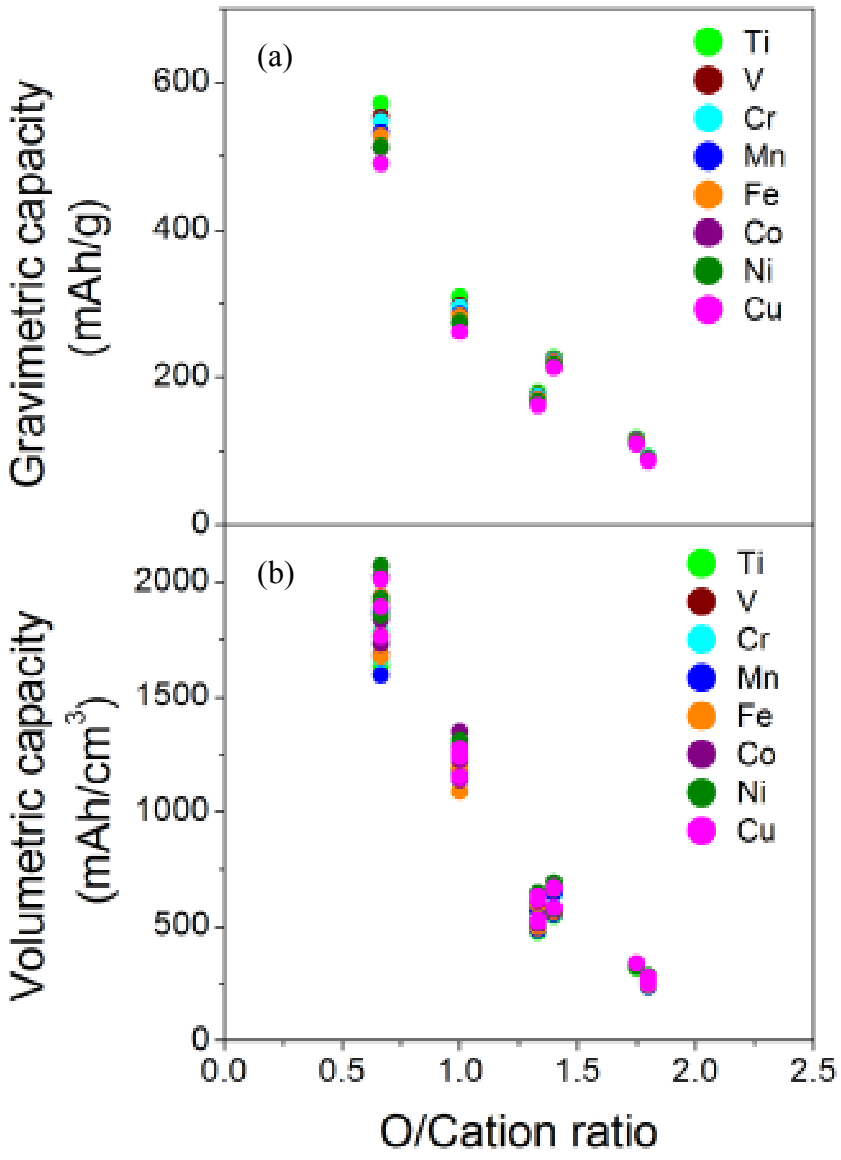

Figure 14 Relationship between O/Cation ratio and (a) gravimetric capacity and (b) volumetric capacity on the lithium transition metal phosphates and lithium transition metal oxides. These capacities are theoretical capacities.

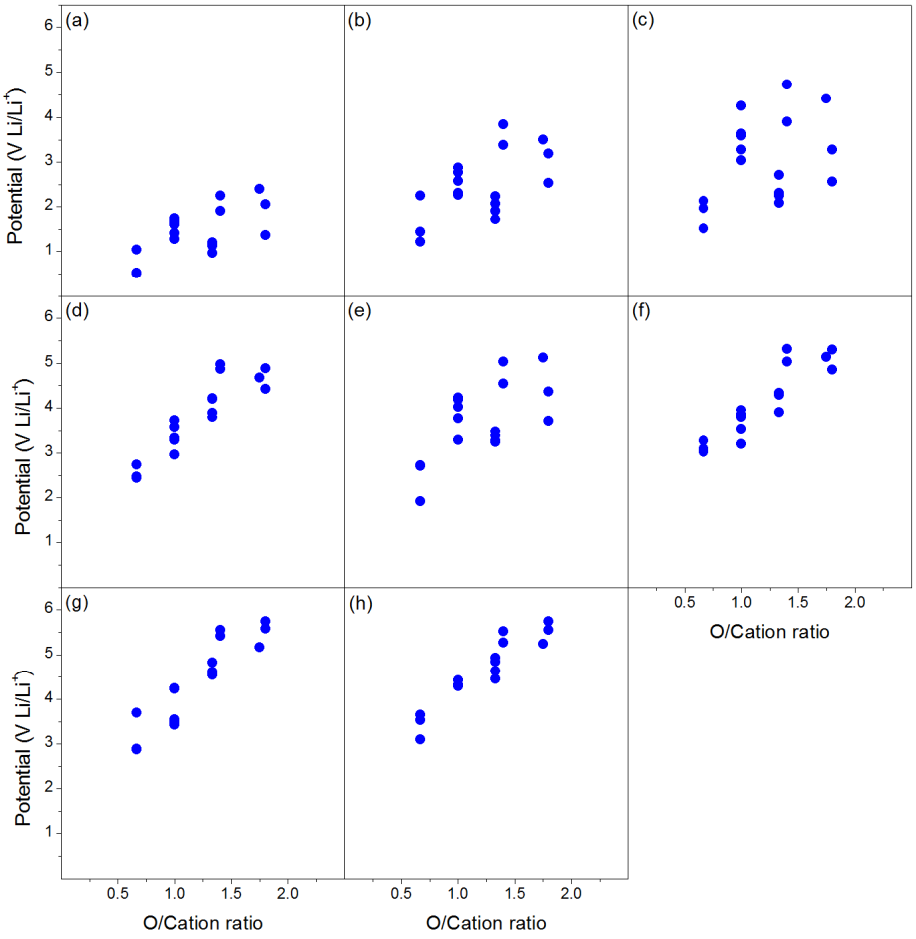

Figure 15 O/Cation ratio vs. redox potential in all calculated compounds, M = (a)Ti, (b)V, (c)Cr, (d)Mn, (e)Fe, (f)Co, (g)Ni and (h)Cu.

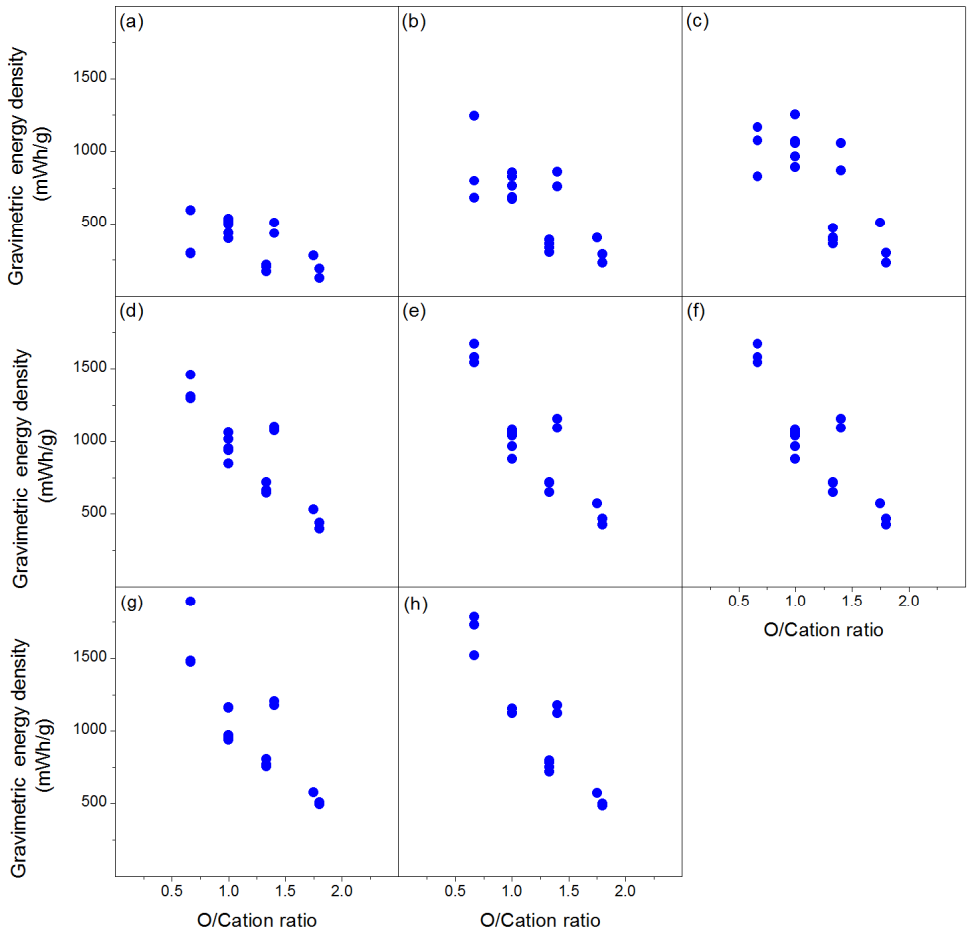

Figure 16 O/Cation ratio vs. gravimetric energy density in all calculated compounds, M = (a)Ti, (b)V, (c)Cr, (d)Mn, (e)Fe, (f)Co, (g)Ni and (h)Cu.

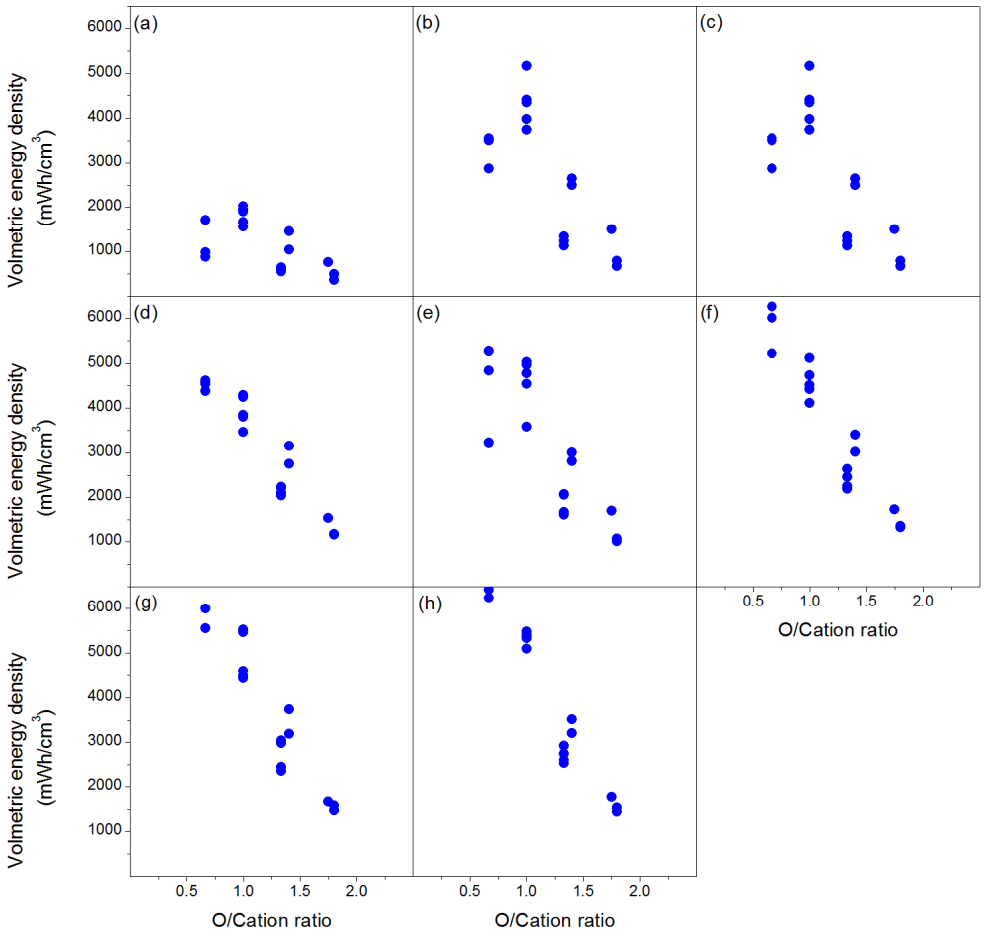

Figure 17 O/Cation ratio vs. volmetric energy density in all calculated compounds, M = (a)Ti, (b)V, (c)Cr, (d)Mn, (e)Fe, (f)Co, (g)Ni and (h)Cu.

4-4 Summary

1. We obtain some relationships between redox potential and structure parameters by a series of first principles calculations.
2. In addition to the species of transition metal elements, O/cation is found to show correlation to the redox potential. The finding would lead to the discovery of new cathode materials in the future considering other factors important for practical applications.
3. A large database can be constructed not only for materials with ground state structures but also for some unstable structures using first principles methods. Such database is hardly constructed merely by experiments. It is therefore very useful for screening of materials.

References

[1] R. A. Leising, M. J. Palazzo, E. S. Takeuchi and K. J. Takeuchi, J. Power Sources, 97–98, 681-683 (2001)

[2] T. Ohsaki, T. Kishi, T.Kuboki, N. Takami, N. Shimura, Y. Sato, M. Sekino and A. Satoh, J. Power Sources, 146(1–2), 97-100 (2005)

[3] Q. Wang, P. Ping, X. Zhao, G. Chu, J. Sun and C. Chen, J. Power Sources, 208(15), 210-224 (2012)

[4] S. Tobishima amd J. Yamaki, J. Power Sources, 81–82, 882-886 (1999)

[5] Y. Baba, S. Okada and J. Yamaki, Solid State Ionics, 148(3–4), 311-316 (2002)

[6] M.M. Thackeray, M.F. Mansuetto, D.W. Dees and D.R. Vissers, Mat. Res. Bulletin, 31(2), 133-140 (1996)

[7] A. S. Andersson,a, J. O. Thomas, B. Kalska and L. Häggströmb, Electrochem. and Solid-State Lett., 3(2), 66-68 (2000)

[8] M. Takahashi, H. Ohtsuka, K. Akuto and Y. Sakurai, Electrochem. Soc., 152(5), A899-A904 (2005)

[9] T. Ohzuku, A. Ueda, and M. Nagayama, J. Electrochem. Soc., 140(7), 1862-1870, (1993)

[10] T. Ohzuku, M. Kitagawa, and T. Hirai, J. Electrochem. Soc., 137(3), 770-775 (1990)

[11] D. Guyomard and J. M. Tarascon, J. Electrochem. Soc., 139(4), 937-948 (1992)

[12] A.K.Padhi, K.S.Nanjundaswamy and J. B. Goodenough, Electrochem. Soc., 144(4), 1188-1194 (1997)

[13] D. Morgan, G. Ceder, M. Y. Saidi, J. Barker, J. Swoyer, H. Huang, G. Adamson. Chem. Mater., 14(11), 4684-4693 (2002).

[14] D. Morgan, G. Ceder, M. Y. Saidi, J. Barker, J. Swoyer, H. Huang and G. Adamson, J. Power Sources, 119, 755-759 (2003).

[15] D. Morgan, A. Van der Ven and G. Ceder, Electrochem. Solid State Lett., 7(2), A30-A32 (2004).

[16] F. Zhou, C.A. Marianetti, M. Cococcioni, D. Morgan and G. Ceder, Phys. Rev. B, 69, 201101 (2004)

[17] F. Zhou, K. Kang, T. Maxisch, G. Ceder and D. Morgan, Solid State Comm., 132, 181-186 (2004)

[18] T. Maxisch, F. Zhou and G. Ceder, Phys. Rev. B, 73, 104301 (2006)

[19] T. Maxisch and G. Ceder, Phys. Rev. B, 73, 174112 (2006)

[20] F. Zhou, T. Maxisch and G. Ceder, Phys. Rev. Lett., 97, 155704 (2006)

[21] L. Wang, F. Zhou, Y.S. Meng and G. Ceder, Phys. Rev. B, 76, 16435 (2007)

[22] S. P. Ong, L. Wang, B. Kang and G. Ceder, Chem. Mater., 20(5), 1798-1807 (2008)

[23] L. Wang, F. Zhou and G. Ceder, Electrochem. Solid-State Lett., 11(6), A94-A96 (2008)

[24] R. Malik, F. Zhou and G. Ceder, Phys. Rev. B, 79, 214201 (2009)

[25] S. P. Ong, A. Jain, G. Hautier, B. Kang and G. Ceder. Electrochem. Comm., 12(3), 427-430 (2010)

[26] S. P. Ong, V. L Chevrier and G. Ceder. Phys. Rev. B, 83(075112), 1-7 (2011)

[27] H. Zhou, S. Upreti, N.A. Chernova, G. Hautierand, G. Ceder and M. S. Whittingham, Chem. Mater., 23(2), 293-300 (2011)

[28] A. Jain, G. Hautier, C. Moore, B. Kang, J. Lee, H. Chen, N. Twu and G. Ceder, J. Electrochem. Soc., 159(5), A622-A633 (2012)

[29] G. Hautier, A. Jain, H. Chen, C. Moore, S. P. Ong and G. Ceder,.J. Mater. Chem., 21, 17147-17153 (2011)

[30] T. Mueller, G. Hautier, A. Jain and G. Ceder, Chem. Mater. A-I (2011).

[31] J. P. Perdew, K. Burke and M. Ernzerhof, Phys. Rev. Letters, 77(18) 3865-3868 (1996)

[32] G. Kresse and J. Furthmuller, Phys. Rev. B, 54(16) 11169-11186 (1996)

[33] P. E. Blochl, Phys. Rev. B, 50(24) 17953-17979 (1994)

[34] V. I Anisimov, F Aryasetiawan and A I Lichtenstein, J. Phys.: Condens. Matter, 9, 767–808 (1997)

[35] V. I. Anisimov, J. Zaanen and O. K. Andersen, Phys. Rev. B, 44(3) 943-954 (1991)

[36] F. Zhou, M. Cococcioni, C. A. Marianetti, D. Morgan, and G. Ceder, Phys. Rev. B, 70, 235121 (2004)

[37] W. Setyawan, R. M. Gaume, S. Lam, R. S. Feigelson and S. Curtarolo, ACS Comb. Sci., 13, 382–390 (2011)

[38] H. J. Monkhorst and J. D. Pack, Phys. Rev. B, 13, 5188 (1976)

[39] G. Ceder, M.K. Aydinol and A.F. Kohan, Comp. Mat. Sci., 8(1–2) 161-169 (1997)

[40] Y. Koyama, I. Tanaka, Y. Kim, S. R. Nishitani, and H. Adachi, J. Appl. Phys., 38, 4804–4808 (1999)

Chapter 5
Conclusion

In this study, we performed a systematic survey of phosphate materials for lithium-ion batteries by first principles calculations. We discussed the phase relationships, crystal structures and redox potentials.

In chapter 2, the phase relationships in pseudo-ternary systems were constructed by the first principle calculations. All compounds were classified into three groups, namely “negative formation energy”, “slightly positive formation energy” and “highly positive formation energy”. The number of compounds with negative formation energy was 63 in calculated compounds given in the ICSD. This result indicates that 62% of calculated compounds given in the ICSD were thermodynamically unstable. Much of the phosphate materials formed thermodynamically unstable structures.

In chapter 3, this work performed the comparative study of crystal structures of lithium metal phosphates. This comparative study used not only thermodynamically stable structures but also thermodynamically unstable structures. Dispersion of the M-O bond length distribution in compounds with negative formation energy was smaller than dispersion of the M-O bond length in compounds with positive formation energy. The M-O bond lengths calculated by first principle calculations did not contradict an experimental data. Li-O bond lengths had wide distribution at each

coordination number and Li-O bond length distributions did not depend on the formation energy. P-O bond length was constant value at all calculated compounds. Nevertheless, all calculated compounds included the thermodynamically unstable compounds. At the phosphates, cell volume was proportional to the phosphorous per cation ratio. If phosphorous per cation ratio is same, the cell volume was proportional to the coordination number of transition metal.

In chapter 4, the redox potential is found to depend not only on species and valence of transition metal but also on cell volume in the lithium transition metal phosphate. The finding would lead to the discovery of new cathode materials in the future considering other factors important for practical applications.

A large database can be constructed not only for materials with ground state structures but also for some unstable structures using first principles methods. Such database is hardly constructed merely by experiments. Combining experimental information, first principles database and data-science techniques would therefore be essential for exploring materials in general. We can expect the daybreak of “materials informatics” very soon.

Acknowledgments

I would like to express my deepest appreciation to Professor Isao Tanaka of Kyoto University for his valuable and constructive suggestions. He gave me an opportunity to take and continue the doctor's course. I also owe a very important debt to Professor Yukinori Koyama of Kyoto University who offered invaluable comments and continuing encouragement. I gratefully acknowledge Professor Fumiyasu Oba and Professor Atsuto Seko of Kyoto University for their technical help. And I would like to thank to all other members in Professor Tanaka's research group.

I am deeply grateful to Dr. Manabu Yamada and Mr. Hiroshi Ueshima of Denso Corporation. They supported to continue the study in the doctor's course. And I would like to thank my colleagues for warm encouragements. I would also like to express my sincere thanks to Dr. Motoaki Nishijima of Sharp Corporation. He gave me an opportunity to take the doctor's course.

Finally I would also like to express my gratitude to my family for their moral support and warm encouragements.